Cell

Dynamics and Memory of Heterochromatin in Living Cells

Nathaniel A. Hathaway,[1,3] Oliver Bell,[1,3] Courtney Hodges,[1] Erik L. Miller,[1,2] Dana S. Neel,[1] and Gerald R. Crabtree[1,*]
[1]Howard Hughes Medical Institute, Department of Developmental Biology and Department of Pathology
[2]Department of Genetics
Stanford University School of Medicine, Stanford, CA 94305, USA
[3]These authors contributed equally to this work
*Correspondence: crabtree@stanford.edu
DOI 10.1016/j.cell.2012.03.052

SUMMARY

Posttranslational histone modifications are important for gene regulation, yet the mode of propagation and the contribution to heritable gene expression states remains controversial. To address these questions, we developed a chromatin in vivo assay (CiA) system employing chemically induced proximity to initiate and terminate chromatin modifications in living cells. We selectively recruited HP1α to induce H3K9me3-dependent gene silencing and describe the kinetics and extent of chromatin modifications at the *Oct4* locus in fibroblasts and pluripotent cells. H3K9me3 propagated symmetrically and continuously at average rates of ~0.18 nucleosomes/hr to produce domains of up to 10 kb. After removal of the HP1α stimulus, heterochromatic domains were heritably transmitted, undiminished through multiple cell generations. Our data enabled quantitative modeling of reaction kinetics, which revealed that dynamic competition between histone marking and turnover, determines the boundaries and stability of H3K9me3 domains. This framework predicts the steady-state dynamics and spatial features of the majority of euchromatic H3K9me3 domains over the genome.

INTRODUCTION

In multicellular organisms, cellular identity is defined by distinct profiles of gene expression that are faithfully transmitted through cell division. There are multiple mechanisms that convey heritable transcriptional information independent of DNA sequence. These epigenetic mechanisms are self-sustaining in the absence of the initial stimulus (Bonasio et al., 2010; Ptashne, 2007). Chemical modifications of DNA and nucleosomal histones have been implicated in contributing to epigenetic programs. However, to date, only DNA methylation has been shown to mediate gene repression that is conserved through cell generations (Goll and Bestor, 2005; Wigler et al., 1981). Some posttranslational histone modifications exhibit strong correlations with transcriptional states (Kouzarides, 2007), and mechanisms for their propagation have been proposed (Margueron et al., 2009; Nakayama et al., 2001; Talbert and Henikoff, 2006). However, genetic approaches have not been able to address the cellular dynamics of chromatin regulation and biochemical approaches have been limited by the inability to faithfully reconstitute chromatin in vitro. Hence, new experimental techniques are required to develop a kinetic understanding of chromatin regulation in living cells.

Position effect variegation (PEV) has been a classical paradigm to study the role of histone modifications in inheritance of transcriptional patterns. In flies, PEV describes a mottled eye phenotype caused by random silencing of the *white* gene when translocated into the proximity of a heterochromatic region (Muller, 1930). Patches of red and white cell clones are maintained through cell divisions in the developing fly eye, indicating that silencing of the *white* gene product is clonally inherited. Genetic screens for PEV modifiers in several organisms have identified multiple proteins implicated in methylation of histone H3 at lysine 9 (H3K9me) (Fodor et al., 2010). In mammalian cells, H3K9 trimethylation (H3K9me3) is a hallmark of heterochromatin (Peters et al., 2002) and is also required for transcriptional silencing of genes and retroviral elements (Magklara et al., 2011; Matsui et al., 2010; Nielsen et al., 2001). Transcriptional repression involves heterochromatin protein 1 (HP1), which specifically binds to methylated H3K9 (Bannister et al., 2001; Lachner et al., 2001; Nakayama et al., 2001). HP1 can form oligomers, which are thought to bridge neighboring nucleosomes and mediate chromatin condensation (Canzio et al., 2011; Verschure et al., 2005). HP1 also directly interacts with and recruits H3K9-specific histone methyltransferases (HMTs) Suv39h1/2 and SETDB1 (Fritsch et al., 2010; Peters et al., 2003; Rea et al., 2000; Schultz et al., 2002). HMT interactions could facilitate self-propagation and sequential methylation of adjacent nucleosomes consistent with a model of linear spreading (Hall et al., 2002; Schotta et al., 2002). Alternatively, it has been suggested that H3K9 methylation could propagate along the chromosome discontinuously through a mechanism of skipping (Talbert and Henikoff, 2006). In *Drosophila*, spreading of heterochromatin depends on the activity and dosage of heterochromatin components and can be antagonized by euchromatic factors (Ebert et al., 2004; Schotta et al., 2002). Although this

competitive balance appears to determine the boundaries of pericentric heterochromatin, it is unclear whether H3K9me3 repressed target genes are also dosage sensitive and subject to dynamic regulation. Moreover, the persistence of the mark at these genes through cell division may be a result of self-propagationor of renewed targeting of HMTs through recruitment by *cis*-regulatory factors after each replication cycle (Moazed, 2011).

We sought to study the formation of heterochromatin at a well-defined euchromatic target promoter in living cells. In embryonic stem (ES) cells, *Oct4* (*Pou5f1*) is highly expressed, encoding a transcription factor that is critical for pluripotency and self-renewal. Upon cellular differentiation, *Oct4* expression is rapidly and completely silenced through a series of events including histone H3K9 methylation, HP1 binding, and DNA methylation (Feldman et al., 2006). Interestingly, in differentiated tissues *Oct4* repression can be overcome by ectopic expression of pluripotency transcription factors (including Oct4 itself), which leads to the formation of pluripotent cells (Takahashi and Yamanaka, 2006). However, cellular reprogramming is highly inefficient, possibly due to repressive chromatin structure that presents a barrier to transcription factor binding.

To investigate the kinetics of chromatin modification and the transmission of epigenetic information, we have generated a murine strain that allows rapid addition and removal of chromatin regulatory activities to a genetically modified *Oct4* allele in any cell type by using small molecule-mediated recruitment. Selective recruitment of HP1α induced H3K9me3 at the *Oct4* reporter locus and subsequent linear spreading in *cis* over a distance of 10 kbp to form a heterochromatic domain with features of PEV. Removal of HP1α from the locus allowed us to study the epigenetic properties of the histone mark, clearly demonstrating that the H3K9me3 domain was inherited through cell divisions in the absence of the initial stimulus. Transcriptional activators could oppose the maintenance of heterochromatin suggesting that the steady state of H3K9me3 is governed by antagonizing activities of histone marking and turnover. Mathematical modeling based on competitive dynamics enabled us to describe the spatial features of heterochromatic domains and to calculate the rates of histone H3K9 methylation and turnover at the *CiA:Oct4* locus in ES cells and fibroblasts. Finally, when applied to genomic data sets, our quantitative framework predicts the steady-state dynamics of the vast majority of all noncentromeric H3K9me3 domains in the mouse genome.

RESULTS

Generation of the Murine Chromatin In Vivo Assay System at *Oct4*

We envisioned an approach where chemically induced proximity (CIP) enables selective addition and removal of different chromatin and transcriptional activities to an endogenous chromosomal locus in vivo (Figure 1). CIP uses bifunctional small molecules that are membrane-permeable and can cause rapid association of two different peptide tags fused to proteins of interest inside cells. Parallel or sequential addition of orthogonal small-molecule ligands has been successfully employed to dissect the mechanism and order of events of various biochemical processes (Graef et al., 1997; Gruber et al., 2006; Ho et al., 1996; Spencer et al., 1993). Importantly, induction of protein proximity is readily reversible in cells or animals by washout or specific displacement using one-sided molecules that bind to only one peptide tag.

Because *Oct4* gene dosage is haplosufficient (Nichols et al., 1998), we genetically modified one *Oct4* allele to recruit chromatin regulators by CIP and to study the effects on gene expression and chromatin structure. We introduced two arrays of different DNA binding sites (12xZFHD1 and 5xGAL4) upstream of the *Oct4* promoter and an in-frame nuclear enhanced green fluorescent protein (EGFP) reporter replacing the first exon of *Oct4* (Figure 1). Targeted ES cells retained good morphology (Figures S1A and S1B available online) and provided real-time fluorescence-based readout of gene expression at single cell resolution. Protein tethering that uses the CIP system involves expression of two sets of chimeric proteins designed to bind different sides of a CIP molecule. The first set is composed of the respective DNA binding domain (GAL4 or ZFHD1) fused to a CIP anchor partner (e.g., FKBP12). The second set of protein chimeras contains the protein of interest fused to the CIP recruitment partner (e.g., FRB). Addition of bifunctional small molecules (e.g., rapamycin) induces the CIP anchor to reversibly bind the CIP recruitment partner, tethering any given protein to the modified *Oct4* allele. We call this system the chromatin in vivo assay (CiA) system and the allele harboring the recruitment domains and reporter at *Oct4*, *CiA:Oct4*.

Nucleosome modifications at the *Oct4* promoter have been well defined in a variety of cell types including mouse ES cells (Figure 1B), where the active gene is modified with histone H3 acetylation (H3ac) and histone H3K4 trimethylation (H3K4me3) (Mikkelsen et al., 2007). In contrast, *Oct4* is transcriptionally repressed in differentiated tissues and packaged into nucleosomes marked by H3K9me3 and H3K27me3. We induced cellular differentiation of CiA ES cells by removal of LIF and treatment with retinoic acid (RA) (Athanasiadou et al., 2010; Sato et al., 2006). Differentiation of CiA ES cells reduced expression of both the endogenous Oct4 protein and the green fluorescent protein (GFP) reporter (Figure S1C). Subsequent chromatin-immunoprecipitation (ChIP) analysis showed that GFP repression was paralleled with a loss of H3K4me3 and gain of repressive H3K9me3 and H3K27me3 (Figure S1D). We concluded that the *CiA:Oct4* allele faithfully reflected physiological regulation of wild-type *Oct4*.

Kinetic Analysis of Heterochromatin Induced by Chemical-Mediated Recruitment

Initiation and maintenance of *Oct4* repression during cellular differentiation involves substantial changes in histone modifications and gain of DNA methylation. To determine the kinetics of H3K9me3-dependent gene repression, we sought to recruit HP1 to the *CiA:Oct4* promoter in ES cells. HP1α is composed of a chromo-domain (CD), which confers specific binding to methylated H3 lysine 9, and a chromo-shadow domain (CSD), which directly interacts with H3K9-specific histone methylases, including SetDB1 and Suv39h1/2 (Hiragami and Festenstein, 2005; Schultz et al., 2002). We infected CiA ES cells with a lentiviral construct of the DNA binding domain of GAL4 (GAL4) fused

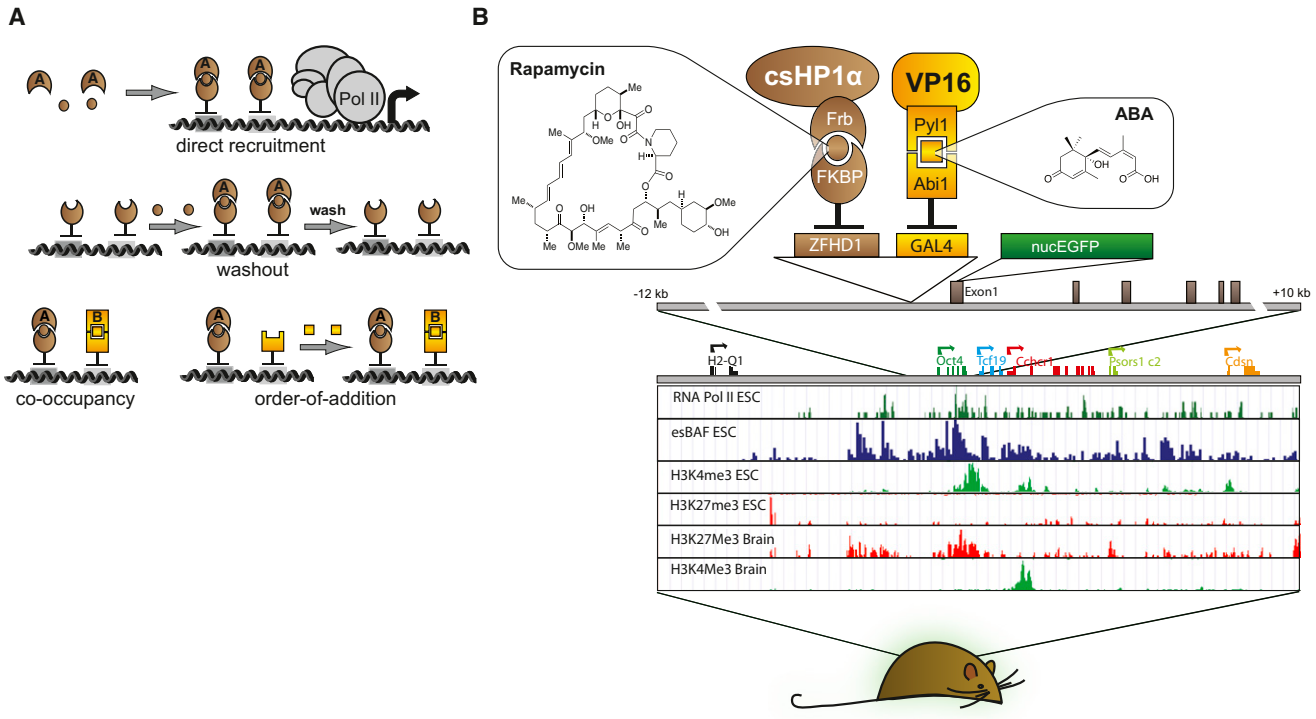

Figure 1. Design of Chromatin In Vivo Assay at *Oct4* (*CiA:Oct4*) ES Cell Line and Mouse

(A) CIP allows direct recruitment, washout, co-occupancy, and order-of-addition experiments.

(B) The *CiA:Oct4* mouse contains one modified *Oct4* allele harboring two arrays of DNA binding sites (12XZFHD1 and 5XGal4) in the promoter region upstream of an in-frame EGFP reporter. Distribution of histone modifications at the *Oct4* locus in murine ES cells and brain tissue (Mikkelsen et al., 2007) reveals the distinct chromatin substrates for CiA modulation.

to either full-length murine HP1α or a truncated form of HP1α containing only the CSD (csHP1α). Although infection with GAL4 alone did not alter GFP, both full-length HP1α and csHP1α fusion proteins induced complete silencing of gene expression as measured by flow cytometry (Figure S1E). To minimize potential nonspecific effects of ectopic HP1α expression, we used csHP1α in subsequent studies.

To gain better temporal resolution of the dynamic processes involved in HP1α-mediated repression, we used the CIP system to recruit csHP1α. We infected CiA ES cells with two lentiviral constructs, one containing GAL4 fused to the CIP anchor, FKBP12, and the other encoding the csHP1α fragment fused to two repeats of the 98 aa FKBP12-rapamycin binding (FRB) domain of mTor with a V5 epitope tag for detection (Figure 2A). After addition of rapamycin, we monitored changes in GFP expression and chromatin structure by flow cytometry and ChIP, respectively. ChIP against the V5 tag revealed significant recruitment of csHP1α within 6 hr and nearly saturated binding within 24 hr after rapamycin addition (Figure 2C). csHP1α targeting led to complete repression of the *CiA:Oct4* reporter within 5 days (Figure 2D). Interestingly, CiA ES cells did not display a gradual decrease in GFP expression but instead segregated into a bimodal population of GFP-positive and GFP-negative cells (Figure 2D, right panel). The distribution and enrichment of histone modifications was determined by ChIP and real-time PCR by using sets of common and reporter allele-specific primers, which cover the distal and proximal regulatory regions upstream and the gene body downstream of the *CiA:Oct4* promoter (Figure 2B). Prior to csHP1α targeting (day 0), H3K27ac was broadly enriched at promoter-distal and -proximal sites, whereas H3K4me3 was only enriched downstream of the active transcription start site (TSS). At this time, H3K9me3 was absent and only basal levels of endogenous HP1γ were detectable (Figure 2D). After 18 hr of csHP1α tethering, we started to observe H3K9me3, which coincided with recruitment of endogenous HP1γ at the *CiA:Oct4* promoter. For the next 4 days, H3K9me3 and HP1γ increased and spread upstream and downstream of the GAL4 binding site. After 5 days of csHP1α recruitment, H3K9me3 had formed a large domain of approximately 10 kbp, which peaked adjacent to the DNA binding site and gradually decreased for 5 kbp to either side (Figure 2D). Interestingly, consistent with the bimodal expression pattern, GFP-negative sorted cells displayed a fully established heterochromatic domain after only 3 days of rapamycin, whereas GFP-positive cells lacked H3K9me3 (Figure S2). This suggests that csHP1α-dependent repression initiates stochastically in an all-or-nothing fashion in individual cells of the population. Gain of H3K9me3 appeared to involve recruitment of SETDB1 (Figure S3A). Loss of active marks and establishment of the H3K9me3 domain did not significantly affect nucleosome

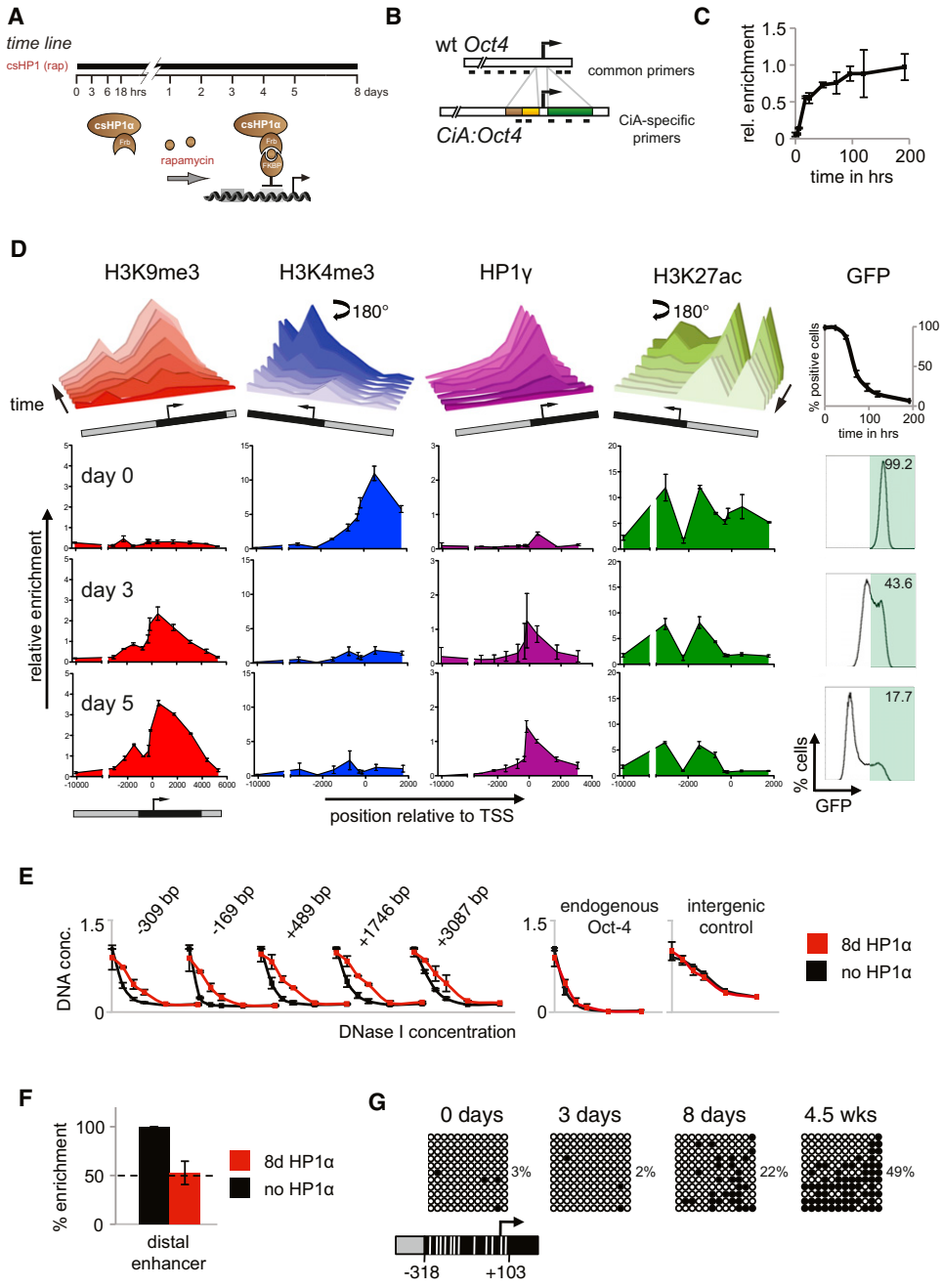

Figure 2. Kinetics of Heterochromatin Formation after HP1α Recruitment in ES Cells

(A) Experimental design: rapamycin addition recruits HP1α chromoshadow fragment (csHP1α) to the *CiA:Oct4* promoter.

(B) Schematic representation of wild-type and CiA alleles depicts location of allele-specific and common real-time PCR primers.

(C) ChIP analysis shows rapamycin-mediated csHP1α recruitment over time.

(D) ChIP analysis reveals dynamic changes of active (H3K4me3, H3K27ac) and repressive (H3K9me3, HP1 gamma) chromatin modifications at the *CiA:Oct4* locus. Upper panel summarizes time course of chromatin remodeling at 0 hr, 24 hr, 48 hr, 72 hr, 96 hr, 120 hr, and 192 hr. Data rotated 180° as indicated to display loss of active marks. Lower panels display ChIP analysis of histone modifications (y axis) across the *CiA:Oct4* locus (x axis) at selected time points. GFP expression was measured by flow cytometry at each time point. Schematic of the reporter allele indicates *CiA:Oct4*-specific primer pairs in black.

(E) DNase I sensitivity across the *CiA:Oct4* locus before and after csHP1α recruitment.

(F) ChIP analysis of Oct4 transcription factor binding at *Oct4* enhancer before and after csHP1α recruitment.

(G) Bisulfite sequencing analysis of DNA methylation changes at the *CiA:Oct4* promoter following csHP1α targeting, with percentage methylated CpGs. White lines in schematic below mark relative positions of CpG dinucleotides.

ChIP and DNase I sensitivity results represent average and SEM of at least two independent experiments. See also Figures S1, S2, and S3.

occupancy at the reporter allele, as measured by total histone H3 ChIP, nor did it alter chromatin structure or expression of the endogenous *Oct4* allele (Figures S3B and S3D).

To test how changes in histone modifications related to chromatin compaction, we analyzed the sensitivity of the *CiA:Oct4* locus to endonuclease digestion. DNase I sensitivity is a hallmark of active promoters, whereas inactive genes and heterochromatic regions are more resistant to digestion (Groudine and Weintraub, 1982; Kerem et al., 1984). We found that the *CiA:Oct4* locus was significantly more resistant to DNase I digestion after 8 days of csHP1α recruitment, whereas DNase I sensitivity remained unaffected at the endogenous *Oct4* promoter as well as at a control locus (Figure 2E). Reduced accessibility to nuclease digestion was also observed at the Oct4 transcription factor binding site located at the distal enhancer 2 kbp upstream of the promoter. PCR primers at this region are outside of the knock-in sequence and thus do not allow discrimination between the endogenous and reporter alleles (Figure 2B). We found that Oct4 binding was reduced by approximately two-fold (Figure 2F). Because Oct4 expression from the wild-type allele is critical for ES cell maintenance, this decline reflected a near-complete eviction of Oct4 protein from the distal enhancer of the *CiA:Oct4* allele.

Upon RA treatment and in differentiated tissues, the *Oct4* promoter is subject to DNA methylation, which has been proposed to stabilize maintenance of gene repression through cell division (Athanasiadou et al., 2010; Feldman et al., 2006). We analyzed levels of CpG methylation at the *CiA:Oct4* promoter during the course of gene silencing. Bisulfite-sequencing revealed low levels of DNA methylation in CiA ES cells prior to csHP1α recruitment. Unlike H3K9me3, DNA methylation was only slightly increased after 8 days when transcription at the locus was fully repressed (Figure 2G). However, promoter methylation continued to gradually increase and was significantly higher at 4.5 weeks, similar to levels found in differentiated cells.

Maintenance of Heterochromatin at the *CiA:Oct4* Locus in ES Cells

We determined the stability of induced heterochromatin and its transmission through cell generations by the timed removal of rapamycin. The *CiA:Oct4* allele was silenced by rapamycin-mediated recruitment of csHP1α for either 7 days or 4.5 weeks followed by rapamycin washout (Figure 3A). We observed comparable levels of H3K9me3 after 7 days or 4.5 weeks (Figure S3F), yet the shorter pulse of csHP1α recruitment induced only low levels of DNA methylation, whereas the extended pulse resulted in high levels of methylation at the *CiA:Oct4* promoter. Although we cannot exclude additional differences, for simplicity, we will refer to the short pulse as "low DNAme" (Figure 2G) and the long pulse as "high DNAme" (Figure 2G). Homogenous populations of GFP-negative cells were obtained by fluorescence-activated cell sorting (FACS) after short (7 days) or long (4.5 weeks) csHP1α treatment. Cells were then passaged in the absence of rapamycin to release csHP1α from the *CiA:Oct4* promoter (Figure 3A). To our surprise, a significant fraction of CiA ES cells began to re-express GFP. CiA ES cells with low DNAme displayed GFP reactivation in 50.7% of the population 4 days after washout and in 63.2% 6 days after washout (Figure 3B). In contrast, only 18.9% of the CiA ES cells with high DNAme displayed GFP reactivation 4 days after washout, and 30.7% after 6 days of washout. To address whether maintenance of GFP repression was controlled by DNA methylation, we treated cells with DNA methyltransferase inhibitor 5-azacytidine (5azaC) (Yoo and Jones, 2006). After a 5azaC pulse for 2 days during washout (days 2–4), GFP repression was rapidly lost regardless of the duration of csHP1α targeting (Figure 3B, lower panel). To test whether increased DNA methylation enhanced heritable repression from one cell generation to the next or whether reactivation of *CiA:Oct4* was stochastic within the population, we followed GFP expression in individual colonies founded by single parental CiA ES cells. GFP-negative cells sorted from low or high DNAme samples were sparsely plated and cultured in the absence of rapamycin for 4 days to form colonies. Colonies were imaged and scored for GFP expression (Figure 3C). Colonies founded by parental cells with low DNAme were 53% GFP-positive or mostly positive, whereas only 10% of colonies were completely GFP-negative. We also observed that many of these colonies contained a mixed population of GFP-positive and -negative cells, indicating that stochastic reactivation occurred in cells with low DNAme. In contrast, colonies formed from high DNAme parental ES cells showed less GFP reactivation. Only 21% of the colonies were GFP-positive, whereas 43% were completely GFP-negative and 21% of the colonies were mostly GFP-negative. These results argue that DNA methylation of the *CiA:Oct4* promoter enhanced maintenance and heritable transmission of gene repression by suppressing spontaneous reactivation in the absence of the HP1 stimulus.

To examine whether the stability of the heterochromatic domain was dependent on DNA methylation, we measured H3K9me3 after 4 days of rapamycin washout and in the presence or absence of 5azaC. Consistent with rapid gain of GFP expression (Figure 3B), cells with low DNAme exhibited a dramatic reduction of H3K9me3 concomitant with an increase in active histone modifications (Figure 3D). CiA ES cells with high DNAme also displayed reduced levels of H3K9me3 and increased H3K4me3. However, these changes were less extensive than in cells with low DNAme. H3K9me3 was rapidly and uniformly lost upon addition of DNA methylation inhibitors 5azaC (Figure 3D).

Activation of the *CiA:Oct4* Locus in Fibroblasts and Dynamics of Re-Establishment of Heterochromatin

To determine whether transcriptional opposition led to H3K9me3 instability, we needed to examine the maintenance of heterochromatin in a tissue lacking ES cell pluripotency factors. We generated a mouse from CiA ES cells and prepared mouse embryonic fibroblasts (MEFs). In these cells, the *CiA:Oct4* allele was transcriptionally silent and embedded in repressive chromatin with high levels of H3K9me3 and H3K27me3 (Figure S4). To erase these repressive marks, we recruited transcriptional activator VP16 to the *CiA:Oct4* promoter. Based on studies of reprogramming, we expected *Oct4* reactivation to require 14–16 days or not to be possible at all. Surprisingly, 24 hr after infection we detected a small fraction of reactivated cells by

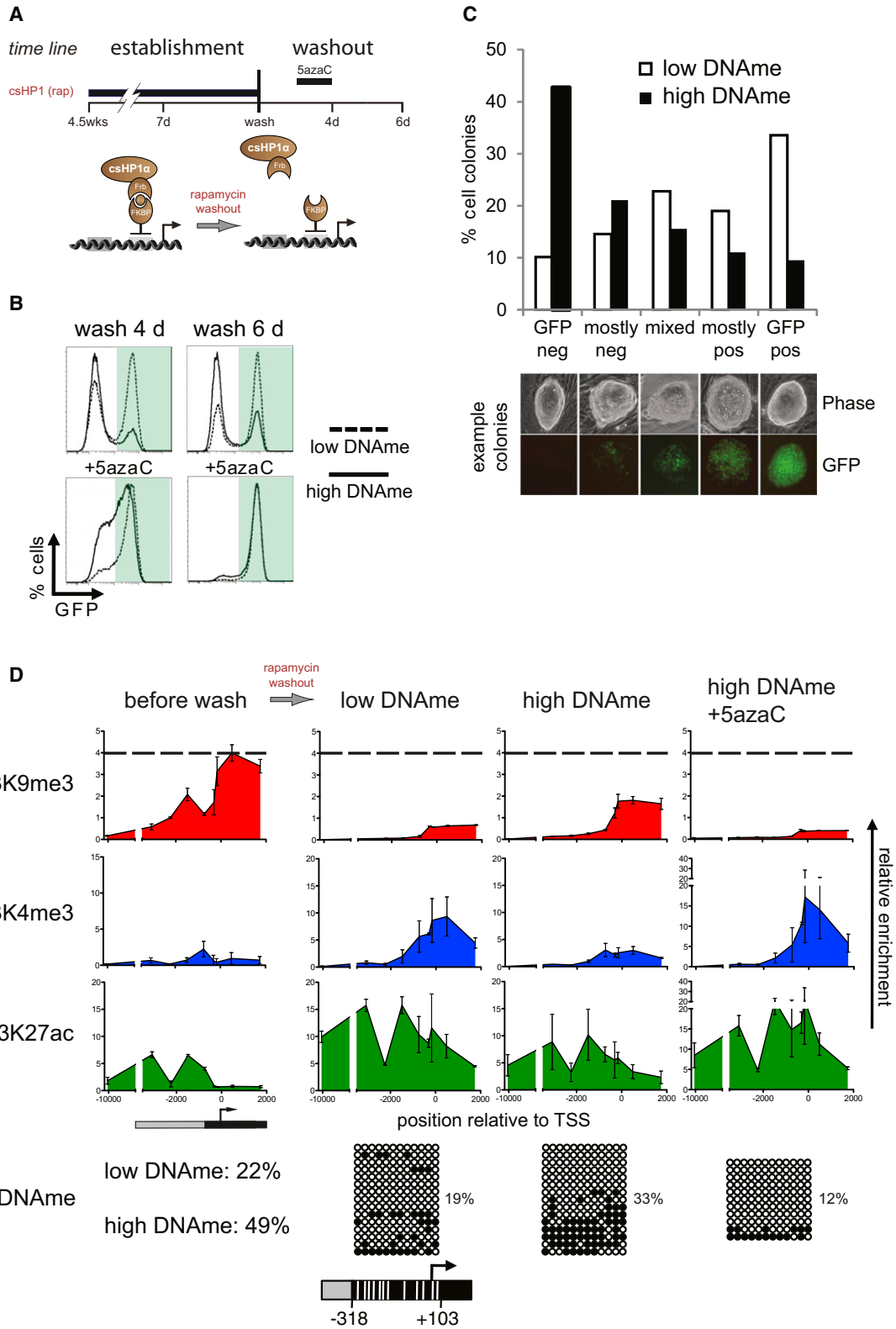

Figure 3. Maintenance of Heterochromatin and Heritable *Oct4* Repression in ES Cells

(A) Experimental design: rapamycin was added for either 7 days or 4.5 weeks and then washed-out with or without Dnmt-inhibitor 5azaC.

(B) Flow cytometry analysis after release from csHP1α after 7 days (low-promoter DNAme) or after 4.5 weeks (high-promoter DNAme).

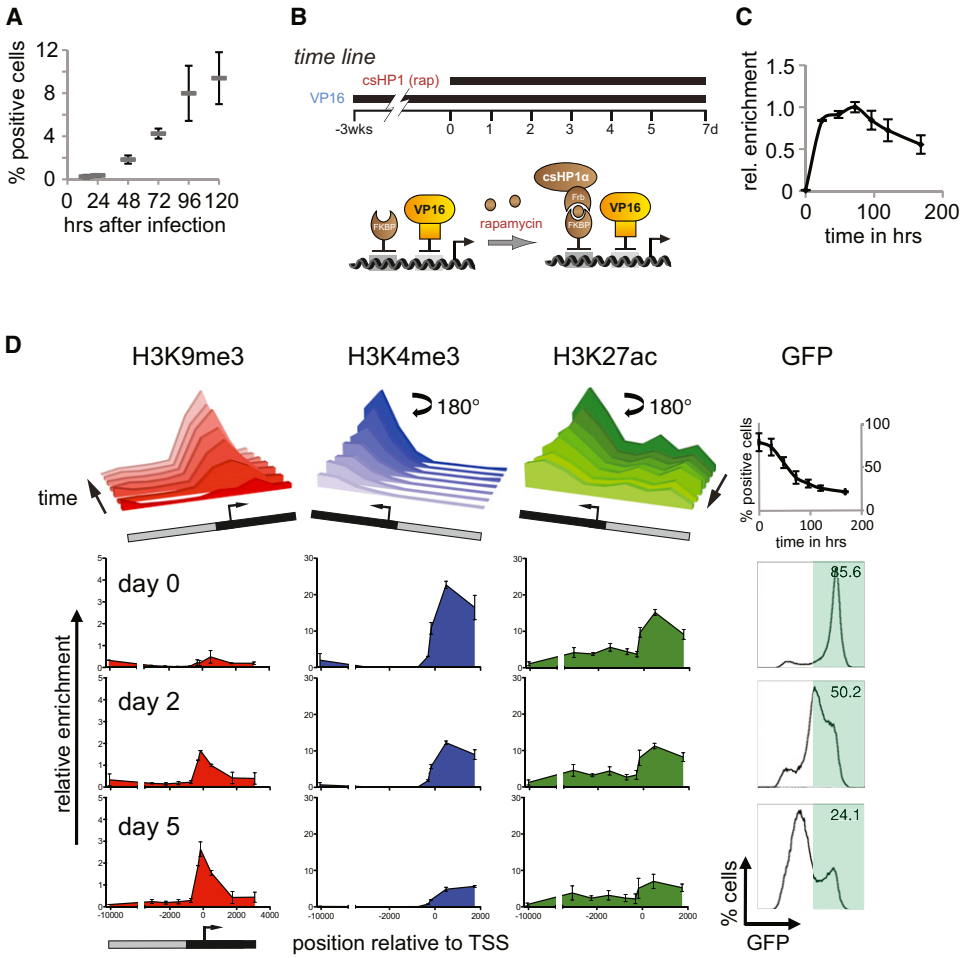

Figure 4. *CiA:Oct4* Activation and Kinetics of Heterochromatin Formation in MEFs

(A) CiA E14.5 p4 MEFs were infected with lentiviral constructs of either GAL4 alone or a GAL4-VP16 fusion. Puromycin was added at 48 hr and cells analyzed by flow cytometry.

(B) Experimental design: the *CiA:Oct4* allele was reactivated by GAL4-VP16 in transformed CiA MEFs. GFP-positive cells were enriched by FACS and treated with rapamycin to induce csHP1α targeting.

(C) ChIP analysis of rapamycin-mediated csHP1α recruitment over time.

(D) ChIP analysis reveals dynamic changes of active (H3K4me3, H3K27ac) and repressive (H3K9me3) histone modifications at the *CiA:Oct4* locus. Upper panel summarizes time course of chromatin remodeling at 0 hr, 24 hr, 48 hr, 72 hr, 96 hr, 120 hr, and 192 hr. Data rotated 180° as indicated to display loss of active marks. Lower panels display loss of active and gain of repressive histone modifications (y axis) across the *CiA:Oct4* locus (x axis) at selected time points. GFP expression was measured by flow cytometry analysis at each time point.

ChIP results represent average and SEM of at least two independent experiments. See also Figures S4 and S5.

flow cytometry, and by 48 hr we observed GFP reactivation in approximately 2% of CiA MEFs (Figure 4A). Five days following infection with GAL4-VP16, nearly 10% of the cell population stably expressed the *CiA:Oct4* reporter. This is an especially high proportion considering that the artificially reactivated reporter allele conferred no competitive growth advantage. These results demonstrate that directed recruitment of a strong transcriptional activator was capable of rapidly reactivating *Oct4* in differentiated cells.

We generated a uniform cell line by transforming CiA MEFs with simian virus 40 large T antigen. We sorted a homogenous population of GFP-positive MEFs and examined the chromatin structure at the *CiA:Oct4* locus. Similar to CiA ES cells, sorted VP16-activated MEFs displayed H3K4me3 and H3K27ac and

(C) Colony growth assay tests heritability of *CiA:Oct4* repression. GFP expression of individual colonies was quantified by microscopy (7 days, n = 158; 4.5 weeks, n = 199).

(D) ChIP analysis of histone modifications after rapamycin washout. The bottom panels depict bisulfite sequencing analysis of DNA methylation at *CiA:Oct4* promoter after csHP1α washout for 4 days. White lines in schematic below mark relative positions of CpG dinucleotides.

ChIP results represent average and SEM of at least two independent experiments.

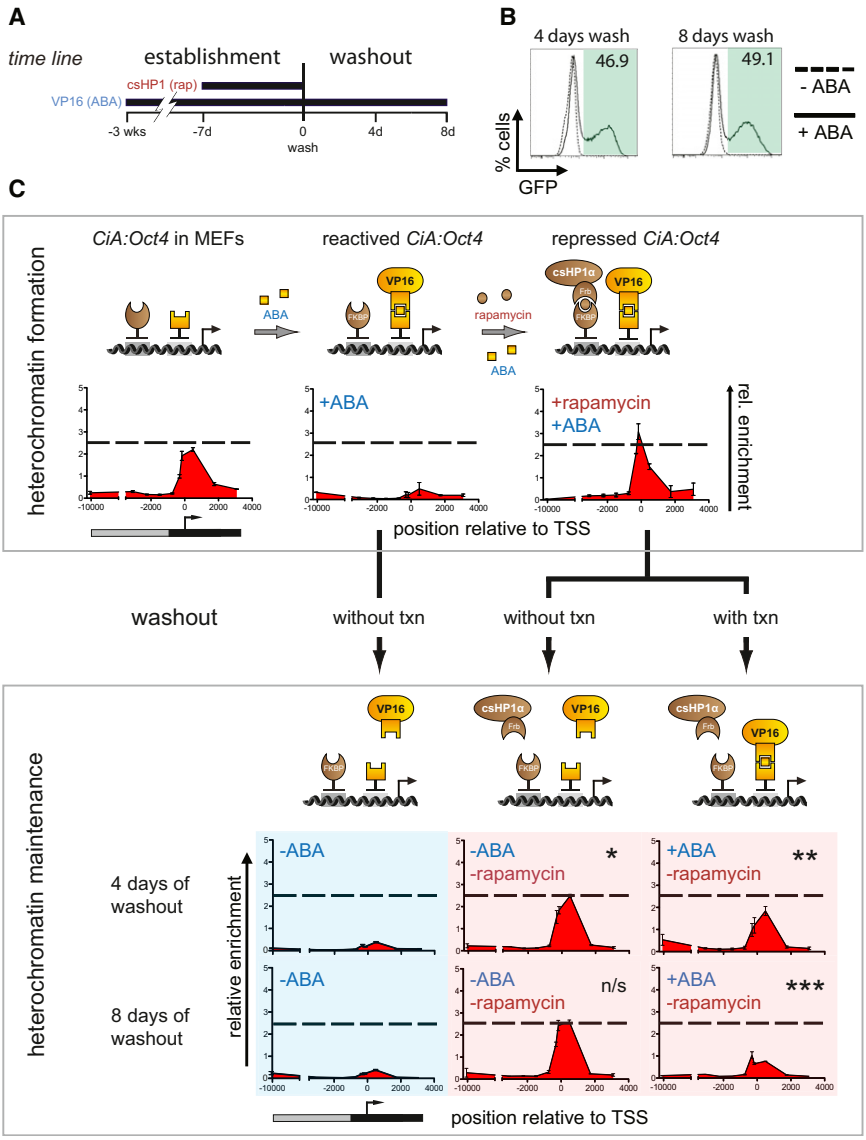

Figure 5. Maintenance of Heterochromatin and Dependence on Transcription

(A) Experimental design: the *CiA:Oct4* allele was reactivated in transformed CiA MEFs by abscisic acid (ABA)-mediated recruitment of VP16. GFP-positive reactivated cells were enriched by FACS. Rapamycin was added for 7 days to recruit csHP1α. GFP-negative cells were sorted by FACS. Finally, rapamycin was washed out in the presence or absence of ABA-recruited VP16. Cells were analyzed four and eight days later.

(B) Flow cytometry analysis after removal of csHP1α in the presence and absence of ABA-recruited VP16.

(C) Cartoon depicts recruitment strategy to form heterochromatin and test its maintenance. ChIP analysis of H3K9me3 along the *CiA:Oct4* allele during heterochromatin formation and after csHP1α removal with or without ABA-mediated VP16 recruitment for 4 and 8 days. H3K9me3 is maintained after rapamycin washout when not opposed by ABA-mediated transcription (p values: *p = 0.052, n/s = not significant, **p = 0.007, ***p = 0.004).

ChIP results represent average and SEM of at least two independent experiments. See also Figure S6.

lacked significant levels of H3K9me3 (Figures S4). The ability to reactivate the *CiA:Oct4* locus allowed us to examine initiation and maintenance of csHP1α-dependent gene repression and compare the dynamics of heterochromatin formation between CiA fibroblasts and ES cells. VP16-activated MEFs were infected with ZFHD1-FKBP12 and csHP1α-2xFRB fusion constructs (Figure 4B). As in CiA ES cells, addition of rapamycin led to rapid csHP1α recruitment within 24 hr (Figure 4C). GFP expression was readily repressed in reactivated CiA MEFs, resembling the overall rate of silencing observed in CiA ES cells (Figures 4D and 2D). However, both the mode of GFP reduction and the formation of heterochromatin were different. In CiA ES cells, csHP1α targeting induced a bimodal transition, whereas a gradual reduction of GFP signal was induced in MEFs (Figures 2D and 4D). During the course of GFP silencing, H3K4me3 and H3K27ac were reduced and H3K9me3 was established (Figure 4D). To examine whether nucleosome displacement during DNA replication was required for the transition from the active to repressed chromatin state, we halted cell division in CiA MEFs by serum starvation. Similar to cycling cells; nondividing cells rapidly silenced GFP expression and established a heterochromatic domain within 5 days of csHP1α tethering (Figure S5). Hence, we conclude that replication-dependent histone exchange was not required for chromatin reprogramming, which may involve replication-independent histone variant incorporation or active demethylation instead. In contrast to CiA ES cells, where the heterochromatic domain covered approximately 10 kbp, the extent of H3K9me3 in both cycling and starved MEF cells was much more constricted, expanding only about 2 kbp at the *CiA:Oct4* promoter (Figures 4D and S5). These data demonstrated that csHP1α targeting could overcome strong transcriptional stimulation by VP16 and induce H3K9me3-dependent repression in MEFs despite forming a smaller heterochromatic domain compared to CiA ES cells.

Heterochromatin Is Stable in the Absence of Transcription at *Oct4*

We sought to address the interplay between transcription and H3K9me3 maintenance by sequential recruitment and removal of the transcriptional activator VP16 in CiA MEFs. We made use of an orthogonal pair of CIP partners, PYL1 and ABI1, which dimerize upon binding of the plant hormone abscisic acid (ABA) (Liang et al., 2011). CiA MEFs were infected with lentiviral constructs containing GAL4-ABI1 and PYL1-VP16 (Figure 5A).

Upon addition of ABA, VP16 was recruited to the CiA locus, resulting in removal of repressive histone modifications and GFP reactivation to a similar extent as the direct fusion of GAL4-VP16 (Figures 4D and 5C). GFP-positive cells were enriched by FACS and maintained consistent GFP expression in the presence of ABA for weeks without defects in growth or morphology. However, within 4 days after ABA removal, more than 99% lost detectable GFP expression and H3K4me3 (Figure S4). Importantly, ChIP analysis did not reveal reemergence of a H3K9me3 domain, indicating that heterochromatin does not form spontaneously without transcription (Figure 5C, blue panel). In this context, the chromatin state of the *CiA:Oct4* locus could be considered as "neutral" for further experimentation on H3K9me3 stability.

Heterochromatin was induced by rapamycin-mediated recruitment of csHP1α for 7 days in VP16-activated CiA MEFs. We then tested H3K9me3 stability through cell division in the absence of the initiating csHP1α stimulus. Rapamycin was removed and cells with or without ABA (recruiting VP16) were analyzed after 4 and 8 days of washout (Figure 5). Unlike in CiA ES cells, H3K9me3 was stably maintained through cell division for at least 8 days following rapamycin washout in absence of ABA (Figure 5C, red panels). H3K9me3 levels remained unchanged even when maintenance of DNA methylation was inhibited with 5azaC (Figure S6). In contrast, upon VP16 recruitment, GFP expression was significantly increased (Figure 5B) and coincided with a reduction of H3K9me3 close to basal levels after 8 days of rapamycin washout. This result indicated that strong transcriptional activation could overcome repressive chromatin structure in the absence of csHP1α tethering similar to our results in CiA ES cells (Figure 5C, red panel). Most importantly however, these results demonstrated that H3K9me3 could be transmitted undiminished through numerous cell divisions in the absence of the initial stimulus.

Model of Heterochromatin Dynamics Reveals In Vivo Rates of Histone Modification

We sought a quantitative model for our observations to rationalize the observed kinetics and spatial distribution of these marks and to define the rates of heterochromatin formation in vivo. One model of histone marking has provided insight into metastable H3K9me switching in the yeast mate-type locus (Dodd et al., 2007). However, this model does not accurately account for the localized peaks and soft borders of the heterochromatic islands observed in our experiments (Figure S7).

We therefore developed a novel and generalizable steady-state kinetic scheme that can be validated by Monte Carlo simulation. We considered the *CiA:Oct4* locus as a one-dimensional lattice, with each lattice position corresponding to an individual nucleosome (full details in Extended Experimental Procedures). We reasoned that H3K9me3 dynamics at a given locus would be governed by processes involved in either addition or removal of the mark. Our general kinetic scheme integrates all processes that propagate H3K9me3 into a single net propagation rate (k_+), and integrates all processes that result in H3K9me3 removal into a separate turnover rate (k_-, see Figure 6A). In our model, k_+ describes the net rate of H3K9me3 addition at nucleosomes adjacent to H3K9me3-marked sites. In this model, H3K9me3 spreading along the chromosome occurs exclusively through linear propagation to neighboring nucleosomes, consistent with our experimental results and the proposed propagation model via HP1 oligomerization (Bannister et al., 2001; Canzio et al., 2011; Hall et al., 2002; Lachner et al., 2001; Schotta et al., 2002). Unlike propagation, we reasoned that turnover of H3K9me3 is equally likely everywhere, thus k_- describes the stochastic turnover of H3K9me3 at any marked nucleosome. In our model, the origin corresponds to the site of csHP1α recruitment; H3K9me3 marks are nucleated at this unique site at rate k_+^{target} in the presence of the CIP (i.e., rapamycin).

Our kinetic model thus describes a single nucleation site, from which H3K9me3 can be placed at rate k_+^{target}, and propagated to neighboring sites at rate k_+. This propagation is opposed by random turnover at rate k_-. According to this scheme, a stochastic, bounded steady-state domain of H3K9me3 centered on the csHP1α nucleation site was established (Figure 6A, right panel). This simple scheme led to the formation of a stable heterochromatic domain, which peaked at the nucleation site and displayed soft continuous borders, consistent with our observations in CiA ES cells and MEFs. Moreover, under these conditions the model predicted a rapid collapse of H3K9me3 upon withdrawal of the initiating stimulus (Figure 6B, lower panel). This was similar to the lack of H3K9me3 maintenance observed in CiA ES cells. Thus, additional mechanisms might be required to support H3K9me3 stability and epigenetic memory. We extended our dynamic competition model of H3K9me3 marking to include an additional transition that stabilized the H3K9me3 state, which we call H3K9me3*. We reasoned that this stabilization process occurs at a slow rate, k^*, and only at sites that are already H3K9me3 modified. In our simulations, this parameter led to sparse transitions to the H3K9me3* state, which prevented H3K9me3 turnover (Figure 6B, upper panel). Importantly, with this feedback mechanism, the H3K9me3 domain was stably maintained even upon withdrawal of the initial stimulus (Figure 6B). We conclude that besides HP1α, additional heritable feedback mechanisms (e.g., lack of transcriptional activators, DNA methylation, or chromatin compaction of the locus) are necessary to ensure epigenetic memory of H3K9me3 silencing.

Next, we determined the cellular modification and turnover rates by comparing our empirical measurements to our model of H3K9me3 marking. Our kinetic model indicated that a restricted domain of H3K9me3 naturally arises from the dynamic competition between marking and turnover when the ratio $\kappa = k_+/k_- \leq 1.5$. At values of $\kappa > 1.5$, the domain of H3K9me3 marks spreads without bounds (Figure 6C). Despite the simplicity of the kinetic scheme, the profiles of the H3K9me3 domains established in simulations under these constraints fit well to our data (Figure 6D). The profile of the H3K9me3 domain in CiA ES cells is best described by $\kappa \sim 1.5$, and in CiA MEFs by $\kappa \sim 1.0$. We conclude that slight differences in the relative rates of propagation or turnover can explain the observation that the H3K9me3 domain is characteristically larger in CiA ES cells.

We then obtained specific values for nucleosome modification and turnover (k_+ and k_-) in each cell type by comparing the empirical rates of H3K9me3 accumulation measured by ChIP. As described above, the ratio κ was obtained by fitting the

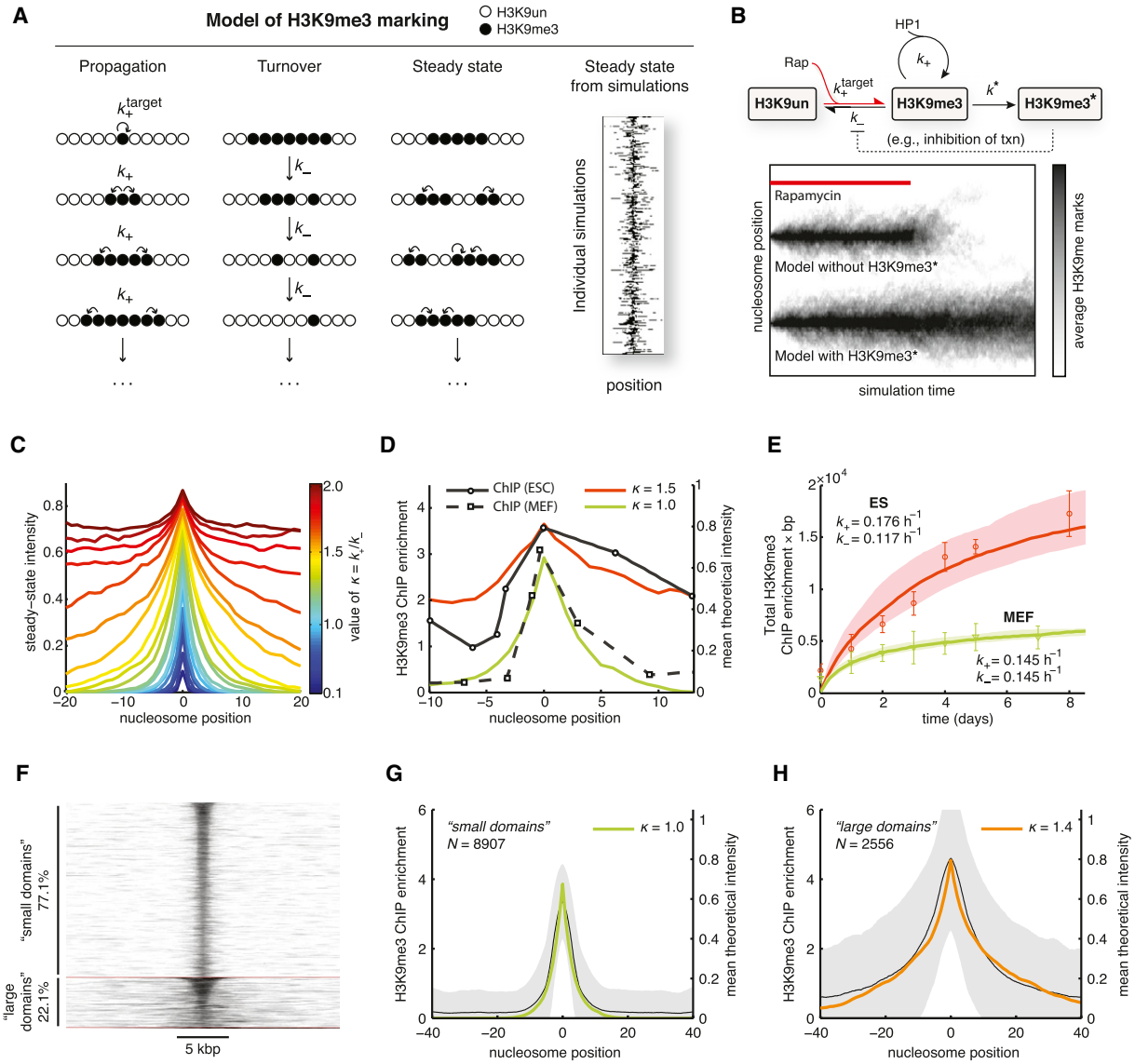

Figure 6. Kinetic Model of H3K9me3 Dynamics

(A) We consider chromatin as a one-dimensional beads-on-a-string lattice. Three processes: nucleation, propagation and turnover, yield a bounded steady-state island of marks. Nucleation occurs at the target site at rate k_+. Propagation of the mark continues at sites immediately adjacent to marked sites, at rate k_+. Turnover of the mark is equally likely everywhere at rate k_-. When these processes are allowed to occur at the same time, a stochastic, bounded island of H3K9me3 marks is established at steady state. Sample output of the model with H3K9me3 domains at steady state (right panel; each horizontal line represents a single simulation).

(B) Simplified kinetic scheme of H3K9me3 dynamics. Without a feedback mechanism to reinforce placement of H3K9me3 marks, the domain collapses in the absence of continued nucleation (lower panel). In the presence of a feedback mechanism that stabilizes H3K9 methylation (denoted by H3K9me3*) the domain persists.

(C) The profile of the steady-state island varies with κ (defined in main text). Larger values of κ increase the size of the island until $\kappa > 1.5$; above this value, the island grows without bounds.

(D) Fits of the experimental H3K9me3 ChIP data shown in Figure 2 to the kinetic model. Data from ES cells are best described by $\kappa = 1.5$, whereas the data from MEFs are described by $\kappa = 1.0$.

(E) Specific values of k_+ and k_- were obtained by fitting the simulations to a time course of integrated H3K9me3 ChIP enrichment at the locus (see Figure 2). Resulting values of k_+ and k_- are shown next to the data for each cell type. Our estimated uncertainty in these values is 35% (shaded regions).

(F) Clustering of genomic H3K9me3 domains in ES cells (Bilodeau et al., 2009) by *k*-means, with $k = 3$. Clustering identified two predominant groups ("small" and "large" H3K9me3 domains), and a very small number of aberrant domains.

(G) Small H3K9me3 domains (mean ± SD) are described well by our model with $\kappa = 1.0$.

(H) Large H3K9me3 domains (mean ± SD) are described well by our model with $\kappa = 1.4$.

See also Figure S7.

simulation profile to the in vivo steady-state H3K9me3 domain (Figure 6D). This ratio constrains the relationship between k_+ and k_-, requiring us only to align the timescale of the simulations to the experimental data to obtain the real rates. To perform this fit, we considered that each simulated nucleosome plus internucleosomal DNA covers a length of 200 bp and integrated our ChIP enrichment values within 3 kbp of the transcription start site. We also used the same relationship between ChIP enrichment and theoretical intensity shown in Figure 6D. We found that the rates k_+ and k_- in ES cells are respectively 0.176 h^{-1} and 0.117 h^{-1}, and in MEFs are respectively 0.145 h^{-1} and 0.145 h^{-1} (Figure 6E). We estimated the uncertainty in these values to be ~35%. Thus, we conclude that H3K9me3 marks propagate along the chromosome, marking neighboring nucleosomes on average every ~5.7 hr in ES cells and every ~6.9 hr in MEFs.

Kinetic Model Predicts Shapes of Genomic H3K9me3 Domains

We next compared the predictions of our H3K9me3 model with previously published H3K9me3 ChIP-seq data from mouse ES cells (Bilodeau et al., 2009). Using *k*-means clustering, we clustered 11,556 H3K9me3 domains into three groups (Figure 6F; full details in Extended Experimental Procedures). This clustering separated the H3K9me3 data into similarly sized "small domains" (8,907; 77.1% of the data), "large domains" (2,556; 22.1%), and a small number of "aberrant domains" (93; 0.8%), which did not fit well in either group.

Within the "large" and "small" H3K9me3 domains, we compared the class averages of H3K9me3 ChIP intensity to our model. The average profiles of both large and small domains displayed localized H3K9me3 peaks with shapes that could be readily fitted to our model. Small H3K9me3 domains were described by $\kappa = 1.0$ (Figure 6G), and large domains fit well with $\kappa = 1.4$ (Figure 6H). Unlike H3K9me3 peaks, H3K36me3 is broadly distributed over active gene bodies forming plateau-shaped domains (Mikkelsen et al., 2007). Genomic H3K36me3 profiles did not cluster well into groups consistent with our model (not shown). We conclude that the general model described above is consistent with the profiles of 99.2% of noncentromeric H3K9me3 domains.

DISCUSSION

Kinetics and Bounding of Heterochromatic Domains

The temporal control achieved with the CiA system provided the motivation to develop a mathematical model of the kinetics and spreading of H3K9me3. We reasoned that at steady-state H3K9me3 is governed by dynamic competition of opposing activities with a rate of addition (k_+) and a rate of H3K9me3 turnover (k_-). Thus, the ratio of these two rates weighs the relative contributions of various cellular processes, including csHP1α recruitment, H3K9 methylation, demethylation, and nucleosomal turnover. Remarkably, by modeling different ratios of these two rates (κ), we identified good fits to the spatial distributions of H3K9me3 in both ES cells and fibroblasts. Based on these results, we were able to define the net rates of H3K9 methylation as well as the turnover rates of modified histones at the *CiA:Oct4* locus in ES cells and fibroblasts. The estimated net turnover rate k_- approximates previously measured rates of global histone turnover in HeLa S3 cells (Zee et al., 2010) and rates of histone H3 displacement from chromatin in *Drosophila* S2 cultures (Deal et al., 2010), supporting the validity of our model (Figure S7). Furthermore, our model suggests that heterochromatic boundaries need not necessarily be limited by local insulator elements. Instead, transitions between heterochromatin and euchromatin might reflect a gradual shift in the balance of activities that add and remove histone modifications. In CiA cells, H3K9me3 marking gradually decreases to either side of the csHP1α recruitment site. According to the model, this is consistent with a reduction in the maintenance of heterochromatin with increasing distance from the initiation site.

In addition to heterochromatin formation at the *CiA:Oct4* locus, our model accounts for endogenous steady-state distribution profiles of H3K9me3 domains throughout the mouse genome. Indeed, an overwhelming majority (99.2%) of noncentromeric H3K9me3 domains can be described well by our model with a single variable parameter. This general parameter, κ, describes the rate of H3K9me3 propagation relative to mark turnover at a given nucleosomal position. Although these individual rates may vary considerably throughout the genome, we find that the value of κ falls within a narrow range for nearly all H3K9me3 domains. This may reflect that H3K9me3 domains are compacted and less accessible, and therefore the turnover rates within the domains are expected to be quite slow. In this case, even modest variation in the propagation rate will result in larger or smaller H3K9me3 domains.

Memory and Propagation of H3K9me3 through Cell Generations

The ability to initiate heterochromatin formation and then to terminate csHP1α recruitment allowed us to examine the epigenetic properties of H3K9me3 through cell division. We found that the stability of H3K9 methylation domains differed between cell types and varied in the context of transcription and DNA methylation. Chemically induced H3K9me3 was stably maintained through cell divisions upon removal of the csHP1α stimulus in CiA MEFs. In the absence of induced transcription, this maintenance did not rely on DNA methylation, as enrichment and extent of H3K9me3 was retained at low levels of promoter methylation and also after 5azaC treatment. However, upon washout of the csHP1α stimulus and recruitment of a potent transcriptional activator, H3K9me3 retention was compromised. The collapse of heterochromatin upon transcriptional activator recruitment resembled the rapid loss of H3K9me3 after washout in CiA ES cells with low DNAme or after treatment with 5azaC. Although GFP reactivation was also detected in ES cells with high DNAme, this population was significantly smaller, suggesting that high levels of DNA methylation could enhance heterochromatin stability in these cells. We conclude that H3K9me3 is an epigenetic mark in the strict sense that it persists after removal of the initial stimulus. However, recruitment of transcriptional activators could disrupt heritable maintenance indicating the reversible nature of this modification. This scenario might occur naturally in the context of signaling-dependent gene activation, in which a transcription factor enters the nucleus to induce transcription and erases a repressive histone mark.

In our model of dynamic competition, maintenance of the heterochromatic domain after rapamycin withdrawal required the establishment of a stabilized state, which we refer to as H3K9me3*. One could imagine that loss of transcriptional activators, gain of DNA methylation, changes in nuclear localization, and/or higher-order chromatin structure may contribute to the increased stability of the H3K9me3* state. Our experiments in MEFs indicated that the absence of transcriptional opposition is an important component of the H3K9me3* state. Along these lines, enhanced H3K9me3 stability in ES cells with high DNAme likely reflects the ability of CpG methylation to interfere with transcriptional activation at the *Oct4* promoter.

Implications for Artificial Modulation of Mammalian Gene Expression Programs

Our model faithfully captures the steady-state dynamics of heterochromatin with the ratio $\kappa = k_+/k_-$, where the opposing effects of histone marking and mark turnover are sufficient to establish an inherently bounded H3K9me3 domain. Synthetic recruitment of the transcriptional activator VP16 to the *CiA:Oct4* locus in MEFs illustrates how disruption of steady-state conditions can compromise the maintenance of chromatin and expression state. In keeping with our model, we speculate that this rapid reactivation reflects a sudden shift in the dynamic balance in favor of k_- due to recruitment of transcriptional machinery. Even in terminally differentiated primary mouse fibroblasts, we observed GFP reactivation within 24 to 48 hr of direct recruitment of VP16 to the *CiA:Oct4* locus. This demonstrates that strong transcription alone can rapidly override the multiple epigenetic mechanisms involved in silencing a single allele.

We demonstrate that the tight temporal control made possible by chemically induced proximity enables quantitative studies in different cell types, which in the future could be extended to different chromatin regulatory mechanisms. Furthermore, the CiA system is adaptable for high-throughput screening for small molecules and natural modifiers of chromatin regulation. Such studies could lead to a better understanding of the mechanisms involved in establishment and maintenance of stable gene expression. We anticipate that integrative models of chromatin dynamics in living cells will be required to understand how gene regulation is achieved through modulation of chromatin structure.

EXPERIMENTAL PROCEDURES

Construction and Culture of Chromatin In Vivo Assay at *Oct4* (*CiA:Oct4*) ES Cells

A BAC containing the mouse *Pou5f1* locus was manipulated through recombineering (see details in Extended Experimental Procedures). Cells were cultured by using standard conditions (see Extended Experimental Procedures).

Generation and Culture of Chromatin In Vivo Assay MEFs

CiA ES cells were injected into Bl/6 derived blastocysts and implanted into surrogate mothers. *CiA:Oct4* allele presence was confirmed by agouti coat color and Southern blot. MEFs were produced and cultured by using standard conditions. See Extended Experimental Procedures for full details.

Construct Design and Chemical Induction of Proximity

All constructs were created in a modified lentivirus backbone with EF1-a promoter driving the gene of interest and a second PGK promoter driving production of a gene resistant to selection. All essential plasmids can be obtained from Addgene. Details on lentiviral production and chemical induction technique in Extended Experimental Procedures.

RA Assay and Western Blots

CiA ES cells were treated with Retinoic Acid at 5 μM for indicated time. Lysates were collected in RIPA buffer (150 mM NaCL, 1% triton, 0.5% sodium deoxycholate, 0.1% SDS, 50 mM Tris pH 8.0). 30 μg/lane total protein was run on 4%–12% Bis-tris gel, transferred to PVDF membranes and imaged by Infrared fluorescence (Li-Cor Biosciences) with the following antibodies: Oct-3/4 (Santa Cruz Biotech, SCBT-9081), GFP (Clontech, 632375), glyceraldehyde 3-phosphate dehydrogenase (GAPDH) (Santa Cruz Biotech, SCBT-32233 or SCBT-25778).

Flow Cytometry Analysis and Sorting

All Flow cytometry analysis was performed on an LSR II (BD Biosciences) and analyzed with FlowJo software, individual cells were gated based on forward and side scatter, autofluorescent cells were omitted, and remaining cells were then analyzed for GFP levels. Cells were sorted by using an Aria or Aria II (BD Biosciences).

ChIP Analysis

ChIP was essentially performed as described previously (Mohn et al., 2008); complete details are in Extended Experimental Procedures. Antibodies used for ChIP are as follows: H3K4me3 (Millipore, 05-745R), H3K27me3 (Millipore, 07-449), H3K9me3 (Abcam, ab8898), H3K27ac (Abcam, ab4729), HP1 gamma (Millipore, 05-690), V5 (Invitrogen, 46-0705), GAL4 (Santa Cruz Biotechnology, sc510), and Oct-3/4 (Santa Cruz Biotech, SCBT-9081). Primers used for real-time PCR listed in Table S1.

Bisulfite Sequencing Analysis of DNA Methylation

One microgram genomic DNA was bisulfite converted with the EpiTec Bisulfite Kit (QIAGEN). Endogenous and knock-in-specific *Oct4* promoter sequences were amplified by PCR and PCR products were cloned by using TOPOTA cloning kit (Invitrogen) followed by sequencing. Methylation profiles were analyzed by using BiQ Analyzer software (Bock et al., 2005). Primers for PCR amplification are listed in Table S1.

DNase I Sensitivity Assay

DNase I sensitivity assay was carried out as previously described (Lu and Richardson, 2004); see Extended Experimental Procedures.

SUPPLEMENTAL INFORMATION

Supplemental Information includes Extended Experimental Procedures, seven figures, and one table and can be found with this article online at doi:10.1016/j.cell.2012.03.052.

ACKNOWLEDGMENTS

We thank D. Schübeler and members of the Crabtree lab, in particular J.L. Ronan and A.S. Koh for insightful comments in the preparation of the manuscript. We gratefully acknowledge technical assistance by L. Chen, A. Kuo, and the Stanford FACS facility. We thank A. Sun, F.S. Liang, and J. Wysocka for sharing reagents. O.B. was supported by EMBO and Human Frontier Science Program fellowships. C.H. is supported by fellowship F32HD072627 from the Eunice Kennedy Shriver National Institute of Child Health and Human Development. Research in the G.R.C. lab is supported by NIH grants (HD55391, NS046789, and AI060037) and the Howard Hughes Medical Institute.

Received: July 2, 2011
Revised: January 5, 2012
Accepted: March 19, 2012
Published online: June 14, 2012

REFERENCES

Athanasiadou, R., de Sousa, D., Myant, K., Merusi, C., Stancheva, I., and Bird, A. (2010). Targeting of de novo DNA methylation throughout the Oct-4 gene regulatory region in differentiating embryonic stem cells. PLoS ONE *5*, e9937.

Bannister, A.J., Zegerman, P., Partridge, J.F., Miska, E.A., Thomas, J.O., Allshire, R.C., and Kouzarides, T. (2001). Selective recognition of methylated lysine 9 on histone H3 by the HP1 chromo domain. Nature *410*, 120–124.

Bilodeau, S., Kagey, M.H., Frampton, G.M., Rahl, P.B., and Young, R.A. (2009). SetDB1 contributes to repression of genes encoding developmental regulators and maintenance of ES cell state. Genes Dev. *23*, 2484–2489.

Bock, C., Reither, S., Mikeska, T., Paulsen, M., Walter, J., and Lengauer, T. (2005). BiQ Analyzer: visualization and quality control for DNA methylation data from bisulfite sequencing. Bioinformatics *21*, 4067–4068.

Bonasio, R., Tu, S., and Reinberg, D. (2010). Molecular signals of epigenetic states. Science *330*, 612–616.

Canzio, D., Chang, E.Y., Shankar, S., Kuchenbecker, K.M., Simon, M.D., Madhani, H.D., Narlikar, G.J., and Al-Sady, B. (2011). Chromodomain-mediated oligomerization of HP1 suggests a nucleosome-bridging mechanism for heterochromatin assembly. Mol. Cell *41*, 67–81.

Deal, R.B., Henikoff, J.G., and Henikoff, S. (2010). Genome-wide kinetics of nucleosome turnover determined by metabolic labeling of histones. Science *328*, 1161–1164.

Dodd, I.B., Micheelsen, M.A., Sneppen, K., and Thon, G. (2007). Theoretical analysis of epigenetic cell memory by nucleosome modification. Cell *129*, 813–822.

Ebert, A., Schotta, G., Lein, S., Kubicek, S., Krauss, V., Jenuwein, T., and Reuter, G. (2004). Su(var) genes regulate the balance between euchromatin and heterochromatin in Drosophila. Genes Dev. *18*, 2973–2983.

Feldman, N., Gerson, A., Fang, J., Li, E., Zhang, Y., Shinkai, Y., Cedar, H., and Bergman, Y. (2006). G9a-mediated irreversible epigenetic inactivation of Oct-3/4 during early embryogenesis. Nat. Cell Biol. *8*, 188–194.

Fodor, B.D., Shukeir, N., Reuter, G., and Jenuwein, T. (2010). Mammalian Su(var) genes in chromatin control. Annu. Rev. Cell Dev. Biol. *26*, 471–501.

Fritsch, L., Robin, P., Mathieu, J.R., Souidi, M., Hinaux, H., Rougeulle, C., Harel-Bellan, A., Ameyar-Zazoua, M., and Ait-Si-Ali, S. (2010). A subset of the histone H3 lysine 9 methyltransferases Suv39h1, G9a, GLP, and SETDB1 participate in a multimeric complex. Mol. Cell *37*, 46–56.

Goll, M.G., and Bestor, T.H. (2005). Eukaryotic cytosine methyltransferases. Annu. Rev. Biochem. *74*, 481–514.

Graef, I.A., Holsinger, L.J., Diver, S., Schreiber, S.L., and Crabtree, G.R. (1997). Proximity and orientation underlie signaling by the non-receptor tyrosine kinase ZAP70. EMBO J. *16*, 5618–5628.

Groudine, M., and Weintraub, H. (1982). Propagation of globin DNAase I-hypersensitive sites in absence of factors required for induction: a possible mechanism for determination. Cell *30*, 131–139.

Gruber, S., Arumugam, P., Katou, Y., Kuglitsch, D., Helmhart, W., Shirahige, K., and Nasmyth, K. (2006). Evidence that loading of cohesin onto chromosomes involves opening of its SMC hinge. Cell *127*, 523–537.

Hall, I.M., Shankaranarayana, G.D., Noma, K., Ayoub, N., Cohen, A., and Grewal, S.I. (2002). Establishment and maintenance of a heterochromatin domain. Science *297*, 2232–2237.

Hiragami, K., and Festenstein, R. (2005). Heterochromatin protein 1: a pervasive controlling influence. Cell. Mol. Life Sci. *62*, 2711–2726.

Ho, S.N., Biggar, S.R., Spencer, D.M., Schreiber, S.L., and Crabtree, G.R. (1996). Dimeric ligands define a role for transcriptional activation domains in reinitiation. Nature *382*, 822–826.

Kerem, B.S., Goitein, R., Diamond, G., Cedar, H., and Marcus, M. (1984). Mapping of DNAase I sensitive regions on mitotic chromosomes. Cell *38*, 493–499.

Kouzarides, T. (2007). Chromatin modifications and their function. Cell *128*, 693–705.

Lachner, M., O'Carroll, D., Rea, S., Mechtler, K., and Jenuwein, T. (2001). Methylation of histone H3 lysine 9 creates a binding site for HP1 proteins. Nature *410*, 116–120.

Liang, F.S., Ho, W.Q., and Crabtree, G.R. (2011). Engineering the ABA plant stress pathway for regulation of induced proximity. Sci. Signal. *4*, rs2.

Lu, Q., and Richardson, B. (2004). DNaseI hypersensitivity analysis of chromatin structure. Methods Mol. Biol. *287*, 77–86.

Magklara, A., Yen, A., Colquitt, B.M., Clowney, E.J., Allen, W., Markenscoff-Papadimitriou, E., Evans, Z.A., Kheradpour, P., Mountoufaris, G., Carey, C., et al. (2011). An epigenetic signature for monoallelic olfactory receptor expression. Cell *145*, 555–570.

Margueron, R., Justin, N., Ohno, K., Sharpe, M.L., Son, J., Drury, W.J., 3rd, Voigt, P., Martin, S.R., Taylor, W.R., De Marco, V., et al. (2009). Role of the polycomb protein EED in the propagation of repressive histone marks. Nature *461*, 762–767.

Matsui, T., Leung, D., Miyashita, H., Maksakova, I.A., Miyachi, H., Kimura, H., Tachibana, M., Lorincz, M.C., and Shinkai, Y. (2010). Proviral silencing in embryonic stem cells requires the histone methyltransferase ESET. Nature *464*, 927–931.

Mikkelsen, T.S., Ku, M., Jaffe, D.B., Issac, B., Lieberman, E., Giannoukos, G., Alvarez, P., Brockman, W., Kim, T.K., Koche, R.P., et al. (2007). Genome-wide maps of chromatin state in pluripotent and lineage-committed cells. Nature *448*, 553–560.

Moazed, D. (2011). Mechanisms for the inheritance of chromatin states. Cell *146*, 510–518.

Mohn, F., Weber, M., Rebhan, M., Roloff, T.C., Richter, J., Stadler, M.B., Bibel, M., and Schübeler, D. (2008). Lineage-specific polycomb targets and de novo DNA methylation define restriction and potential of neuronal progenitors. Mol. Cell *30*, 755–766.

Muller, H. (1930). Types of visible variations induced by X-rays in *Drosophila*. J. Genet. *22*, 299–334.

Nakayama, J., Rice, J.C., Strahl, B.D., Allis, C.D., and Grewal, S.I. (2001). Role of histone H3 lysine 9 methylation in epigenetic control of heterochromatin assembly. Science *292*, 110–113.

Nichols, J., Zevnik, B., Anastassiadis, K., Niwa, H., Klewe-Nebenius, D., Chambers, I., Schöler, H., and Smith, A. (1998). Formation of pluripotent stem cells in the mammalian embryo depends on the POU transcription factor Oct4. Cell *95*, 379–391.

Nielsen, S.J., Schneider, R., Bauer, U.M., Bannister, A.J., Morrison, A., O'Carroll, D., Firestein, R., Cleary, M., Jenuwein, T., Herrera, R.E., and Kouzarides, T. (2001). Rb targets histone H3 methylation and HP1 to promoters. Nature *412*, 561–565.

Peters, A.H., Mermoud, J.E., O'Carroll, D., Pagani, M., Schweizer, D., Brockdorff, N., and Jenuwein, T. (2002). Histone H3 lysine 9 methylation is an epigenetic imprint of facultative heterochromatin. Nat. Genet. *30*, 77–80.

Peters, A.H., Kubicek, S., Mechtler, K., O'Sullivan, R.J., Derijck, A.A., Perez-Burgos, L., Kohlmaier, A., Opravil, S., Tachibana, M., Shinkai, Y., et al. (2003). Partitioning and plasticity of repressive histone methylation states in mammalian chromatin. Mol. Cell *12*, 1577–1589.

Ptashne, M. (2007). On the use of the word 'epigenetic'. Curr. Biol. *17*, R233–R236.

Rea, S., Eisenhaber, F., O'Carroll, D., Strahl, B.D., Sun, Z.W., Schmid, M., Opravil, S., Mechtler, K., Ponting, C.P., Allis, C.D., and Jenuwein, T. (2000). Regulation of chromatin structure by site-specific histone H3 methyltransferases. Nature *406*, 593–599.

Sato, N., Kondo, M., and Arai, K. (2006). The orphan nuclear receptor GCNF recruits DNA methyltransferase for Oct-3/4 silencing. Biochem. Biophys. Res. Commun. *344*, 845–851.

Schotta, G., Ebert, A., Krauss, V., Fischer, A., Hoffmann, J., Rea, S., Jenuwein, T., Dorn, R., and Reuter, G. (2002). Central role of Drosophila SU(VAR)3-9 in histone H3-K9 methylation and heterochromatic gene silencing. EMBO J. *21*, 1121–1131.

Schultz, D.C., Ayyanathan, K., Negorev, D., Maul, G.G., and Rauscher, F.J., 3rd. (2002). SETDB1: a novel KAP-1-associated histone H3, lysine 9-specific methyltransferase that contributes to HP1-mediated silencing of euchromatic genes by KRAB zinc-finger proteins. Genes Dev. *16*, 919–932.

Spencer, D.M., Wandless, T.J., Schreiber, S.L., and Crabtree, G.R. (1993). Controlling signal transduction with synthetic ligands. Science *262*, 1019–1024.

Takahashi, K., and Yamanaka, S. (2006). Induction of pluripotent stem cells from mouse embryonic and adult fibroblast cultures by defined factors. Cell *126*, 663–676.

Talbert, P.B., and Henikoff, S. (2006). Spreading of silent chromatin: inaction at a distance. Nat. Rev. Genet. *7*, 793–803.

Tiscornia, G., Singer, O., and Verma, I.M. (2006). Production and purification of lentiviral vectors. Nat. Protoc. *1*, 241–245.

Verschure, P.J., van der Kraan, I., de Leeuw, W., van der Vlag, J., Carpenter, A.E., Belmont, A.S., and van Driel, R. (2005). In vivo HP1 targeting causes large-scale chromatin condensation and enhanced histone lysine methylation. Mol. Cell. Biol. *25*, 4552–4564.

Wigler, M., Levy, D., and Perucho, M. (1981). The somatic replication of DNA methylation. Cell *24*, 33–40.

Yoo, C.B., and Jones, P.A. (2006). Epigenetic therapy of cancer: past, present and future. Nat. Rev. Drug Discov. *5*, 37–50.

Zee, B.M., Levin, R.S., Dimaggio, P.A., and Garcia, B.A. (2010). Global turnover of histone post-translational modifications and variants in human cells. Epigenetics Chromatin *3*, 22.

EXTENDED EXPERIMENTAL PROCEDURES

Construction and Culture of Chromatin In Vivo Assay at Oct4 (CiA:Oct4) ES Cells

A BAC containing the mouse *Oct4* (*Pou5f1)* locus was manipulated through recombineering. The construct was flanked with homology arms of approximately 3.7 kbp upstream and 10.9 kbp downstream. Two distinct DNA binding sequence arrays were added at −277 bp upstream of the TSS of *Oct4*, 12 x ZFHD1 (TAATGATGGGCG) and 5 x Gal4 (CGGAGTACTGTCCTCCGAG). A nuclear EGFP was inserted at the ATG of exon 1 of *Oct4*, exons 2–5 were deleted after insertion avoid expression of endogenous *Oct4* from the reporter allele. A floxed neomycin resistance cassette was inserted behind the EGFP reporter for positive selection and thymidine kinase was inserted behind the homology arms for negative selection.

All ES cells were grown on gelatin coated dishes in high-glucose DMEM (Invitrogen, 11960) supplemented with ESC-Sure FBS (Applied Stemcell, ASM-5007), 10 mM HEPES pH 7.5, NEAA, glutaMAX, Na Pyruvate, Pen/Strep, 2-Mercaptoethanol, and 1:500 LIF conditioned media produced from Lif −1Cα (COS) cells. Early passage TC1 cells were used for targeting. 1×10^7 cells were electroporated with 20 μg DNA, cells were selected with 400 μg/ml G418 and 1 μM gancyclovir. Colonies were picked and examined by Southern blot for presence of an additional EcoRI site inserted after the EGFP in the targeting construct. Two separate transfections were performed with recombination frequency of 2/288 and 1/168. CiA cells were adapted for growth without the use of feeders for all experiments and typically passaged at a density of $4–5 \times 10^6$ cells per 10 cm plate, split every 2–3 days.

Generation and Culture of Chromatin In Vivo Assay Mouse Embryo Fibroblasts

The presence of the *CiA:Oct4* allele was determined by PCR using the following primers specific to the *CiA:Oct4* knock-in locus: forward (CTAGAGGATCCGAGGACCAATTG) and reverse (AATCCCACCCTCTAGCCTTG). MEF cell lines were generated from F2 pups at embryonic day E14.5 and grown in high-glucose DMEM (Invitrogen, 11960) supplemented with FBS (Omega Scientific, FB-11), 10 mM HEPES pH 7.5, Minimal AA, glutaMAX, Na Pyruvate, Pen/Strep, 2-Mercaptoethanol. Initial reactivation experiments in Figure 4B were conducted on p4 primary MEF lines. To generate a more rapidly proliferating and uniform population of cells for subsequent experiments, MEFs were transformed with a lentivirus harboring the simian virus 40 large T antigen.

Chromatin Immunoprecipitation Analysis

Briefly, for each 10 cm plate sample: cells were trypsinized for 5–8 min, trypsin was quenched by addition of 10 ml media containing FBS, cells were diluted to 40 ml with PBS cells were fixed for 12 min by addition of formaldehyde to a final concentration of 1%, cells, crosslinking was then quenched by addition of 2.5 M glycine (0.125 M final concentration) and cells were then incubated on ice. Crosslinked cells were spun at 600 × *g* for 5 min, nuclei were prepared by consecutive washes with Paro Rinse 1 buffer (10 mM Tris pH 8.0, 10 mM EDTA [pH 8.0], 0.5 mM EGTA, 0.25% Triton X-100) followed by Paro 2 buffer (10 mM Tris pH 8.0, 1 mM EDTA, 0.5 mM EGTA, 200 mM NaCl). Pellets were resuspended in 2 ml total volume of ChIP lysis buffer (50 mM HEPES/KOH pH 7.5, 300 mM NaCl, 1 mM EDTA, 1% Triton X-100, 0.1% DOC, 0.1% SDS, 1× protease inhibitors complete mini (Roche)) and then sonicated for 9 × 30 s (ES cells) or 23 × 30 s at an amplitude of 30 with a Misonix sonicator, or until DNA was sheared to between 500 and 1000 bp (as confirmed by agarose gel).

Dnase I Sensitivity Assay

Dnase I sensitivity assay was carried out essentially as described by Lu and Richardson (2004). Briefly, ES cells were lysed in Dnase I buffer (final 10 mM HEPES [pH 7.5], 50 mM KCl, 5 mM $MgCl_2$, 3 mM $CaCl_2$, 0.1% NP40, 8% Glycerol, 1 mM DTT) and intact nuclei were isolated by using a dounce homogenizer. 200 μl of 1.25×10^7 nuclei/ml were digested at 37°C for exactly 3 min with increasing concentrations of Dnase I (Worthington Biochem. Corp. LS006331). The digestion reaction was terminated with Stop buffer (20 mM EDTA, 1% SDS) followed by treatment with 2 μl RNase A (10 mg/ml) for 1 hr at 37°C and 2 μl of Proteinase K (10 mg/ml) at 55°C overnight. DNA was extracted and concentration was adjusted to 50 ng/μl for subsequent PCR analysis.

Construct Design and Chemical Induction of Proximity

Selection of lentiviral construct achieved with either: puromycin (used at 1.5 ug/ml in ES cells or 3 mg/ml in MEFs), blasticidin (used at 7.5 ug/ml in ES cells or 10 ug/ml in MEFs), or hygromycin (used at 400 μg/ml in MEFs). Lentivirus was produced by PEI (Polysciences Inc., 24765) transfection of 293t lentiX cells (Clontech) with gene delivery vector co-transfected with packaging vectors pspax2 and pMD2.G essentially as described by (Tiscornia et al., 2006). DNA binding domain (GAL4 or ZFHD1) was fused directly to indicated activity or to anchor CIP protein (FKBP12 for CIP with rapamycin or ABA1 for CIP with abscisic acid). Activity of interest as indicated in figures fused to two tandem repeats of Frb (for Rapamycin-mediated recruitment) or PYL1 (for ABA-mediated recruitment). Proximity was induced by addition of rapamycin at 3 nM (final concentration) or ABA at 250 nM (final concentration) in all experiments. For the first 24 hr of rapamycin washout 100 nM FK506 were added to the washout media to more rapidly dissociate rapamycin from FKBP.

List of Plasmids Deposited to Addgene

N111 nLV Dual Promoter EF-1a-MCS-PGK-Puro Gal4-HP1a FL
N112 nLV Dual Promoter EF-1a-MCS-PGK-Puro Gal4-HP1a CS
N113 nLV Dual Promoter EF-1a-Gal4-Stop-PGK-Puro

N114 nLV Dual Promoter EF-1a-Gal4-VP16-PGK-Puro
N118 nLV Dual Promoter EF-1a-Gal-FKBPx1-HA-PGK-Blast
N163 nLV Dual Promoter EF-1a-Hp1a(CS)-Frbx2(Frb+FrbWobb)-V5-PGK-Puro
N205 nLV Dual Promoter EF-1a-ZFHD1-link-FKBP-HA ⟨ T2A ⟩ HP1aCS-Frbx2-V5-PGK-Blast
N168 Oct4 Targeting Vector Used to make CiA:Oct4 ES cell line and mouse

Monte Carlo Simulations

For all simulations, we considered a chromatin region of 256+1 nucleosomes, corresponding to ~50 kbp of DNA if each nucleosome and internucleosomal DNA occupied 200 bp of DNA. Each nucleosome is considered as a discrete position along a one-dimensional lattice.

Marking and turnover are considered as Poisson processes described by the rates k_+ and k_-, respectively. The target site at the center is H3K9 methylated at rate k_+ upon recruitment of GAL4-csHP1a when rapamycin is present. In addition, having an H3K9me mark at any given site causes marking of both neighboring sites at rate k_+, consistent with local recruitment and propagation of HP1. All nucleosomes are subject to loss of the H3K9me mark at rate k_-.

All simulations were allowed to evolve under these rules using periodic boundary conditions, thus the simulations have no natural boundary elements. Either 64 or 128 simulations were run under each condition for 32,768 time steps and averaged at each time step to give the data plotted in Figure 6. At each time step, the acceptance probability for H3K9me turnover (k_-) was 0.05 at each nucleosome, and the acceptance probability for H3K9me propagation (k_+) was varied between 0.005 and 0.15.

Obtaining Specific Values of k_+ and k_-

For Figure 6E, we integrated all ChIP enrichment values by using primer sets between −3077 and +3087 bp of the CIAO reporter's TSS. Integration was performed at each experimental time point by using the rectangle method based on the midpoints between each primer set. The simulation data was integrated at each simulation time step assuming that each nucleosome contains 200 bp of DNA, and presented at the corresponding intensity scale obtained in Figure 6D. Theoretical curves were aligned with the experimental data by finding the time scaling factor that related simulation time to experimental time. The optimal fit was obtained separately for ES cells and MEFs by least-squares minimization.

Analysis of Histone Mark Covariance by ChIP

ChIP enrichment values were obtained for H3K9me3, H3K4me3 and H3K27ac at the CIAO locus at following time points: before addition of rapamycin (0 hr), +3 hr, +6 hr, +18 hr, +1 day, +2 day, +3 day, +4 day, +5 day, and +8 day after addition of rapamycin. Covariance of the histone marks was analyzed by obtaining Pearson correlation coefficients for pairs of marks (e.g., H3K4me3 and H3K9me3) for each ChIP primer set.

As in the text, we report here the mean Pearson correlation coefficient R at the CIAO locus obtained from knockin-specific ChIP primer sets, along with the mean p value:

ES cells
H3K9me3 and H3K4me3, R = -0.923, $p = 2.1 \times 10^{-4}$
H3K27ac and H3K4me3, R = 0.983, $p = 4.4 \times 10^{-7}$
H3K9me3 and H3K27ac, R = -0.937, $p = 1.1 \times 10^{-4}$
MEF cells
H3K9me3 and H3K4me3, R = -0.876, $p = 2.7 \times 10^{-2}$
H3K27ac and H3K4me3, R = 0.906, $p = 6.7 \times 10^{-3}$
H3K9me3 and H3K27ac, R = -0.876, $p = 2.7 \times 10^{-2}$

Statistical Analysis of H3K9me3 ChIP Enrichment

To compare the abundance of H3K9me3 marks at the CiA locus, we summed the ChIP enrichment values across the locus for each replicate and performed a two-sample t test on these sums. The center positions of each primer set relative to the transcription start site were

−3077, −2241, −1485, −739, −308.5, −168.5, 488.5, 1745.5, and 3087 bp.

K-Means Clustering of H3K9me3 and H3K36me3 ChIP-Seq Data Sets

Previously published ChIP-seq data sets acquired for H3K9me3 (Ab8898) (Bilodeau et al., 2009) and H3K36me3 (Mikkelsen et al., 2007) were used for deriving class averages following K-means cluster analysis. K-means clustering by using k = 3 was done on ChIP-seq fragment density across islands of enrichment, as annotated by the original authors and then aligned by their centers, by 25 bp intervals.

SUPPLEMENTAL REFERENCES

Bilodeau, S., Kagey, M.H., Frampton, G.M., Rahl, P.B., and Young, R.A. (2009). SetDB1 contributes to repression of genes encoding developmental regulators and maintenance of ES cell state. Genes Dev. *23*, 2484–2489.

Deal, R.B., Henikoff, J.G., and Henikoff, S. (2010). Genome-wide kinetics of nucleosome turnover determined by metabolic labeling of histones. Science *328*, 1161–1164.

Dodd, I.B., Micheelsen, M.A., Sneppen, K., and Thon, G. (2007). Theoretical analysis of epigenetic cell memory by nucleosome modification. Cell *129*, 813–822.

Lu, Q., and Richardson, B. (2004). DNaseI hypersensitivity analysis of chromatin structure. Methods Mol. Biol. *287*, 77–86.

Mikkelsen, T.S., Ku, M., Jaffe, D.B., Issac, B., Lieberman, E., Giannoukos, G., Alvarez, P., Brockman, W., Kim, T.K., Koche, R.P., et al. (2007). Genome-wide maps of chromatin state in pluripotent and lineage-committed cells. Nature *448*, 553–560.

Zee, B.M., Levin, R.S., Dimaggio, P.A., and Garcia, B.A. (2010). Global turnover of histone post-translational modifications and variants in human cells. Epigenetics Chromatin *3*, 22.

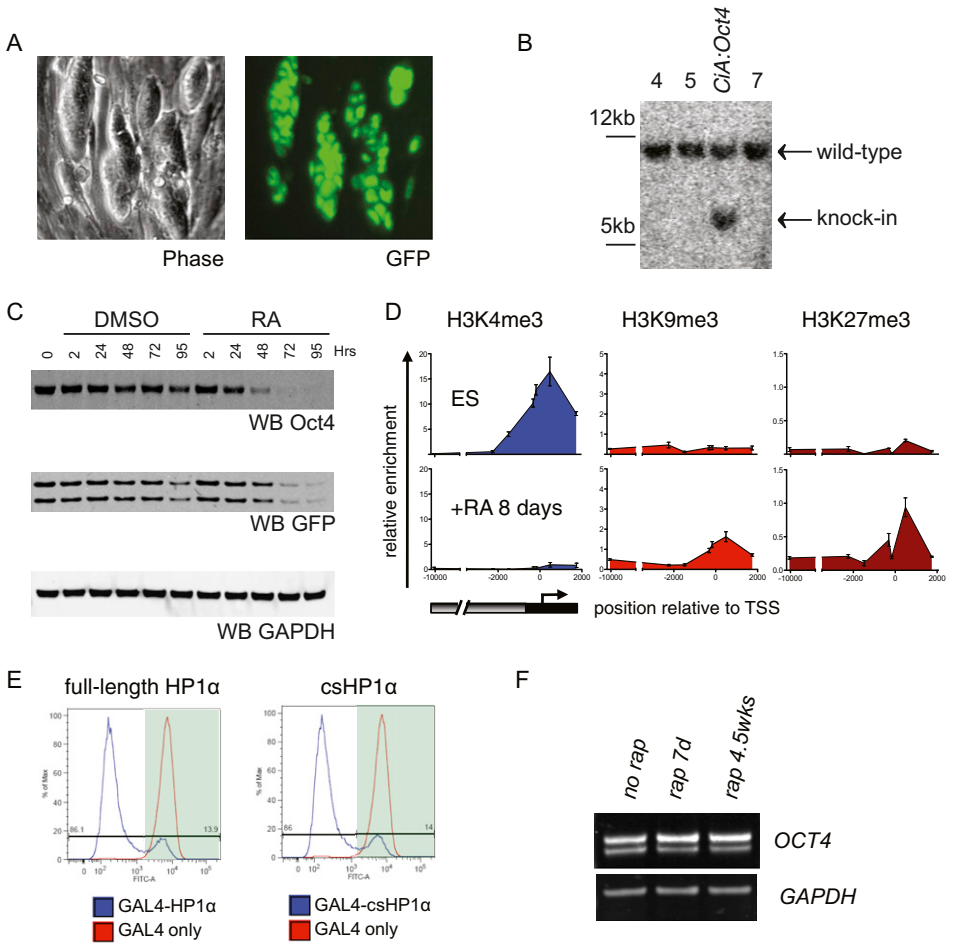

Figure S1. Expression and regulation of the Oct4 reporter in CiA ES cells, Related to Figure 2

(A) Phase contrast and fluourescent image of CiA ES cells demonstrate uniform nuclear GFP expression of the *CiA:Oct4* reporter.

(B) Southern blot analysis confirms single targeting to generate CiA ES cells with one wild-type and one knock-in allele of *Oct4*.

(C) Western blot analysis of Oct4 and GFP protein expression in CiA ES cells before and after 8 days of RA differentiation.

(D) ChIP analysis of histone modifications in CiA ES cells before and after 8 days of RA differentiation. Shown is an average of at least two experiments.

(E) Flow cytometry compares GFP expression upon recruitment of GAL4 fusions with full-length HP1α and csHP1α.

(F) Western blot analysis compares endogenous levels of Oct4 protein expression before and after 7 days and 4.5 weeks of rapamycin treatment in CiA ES cells.

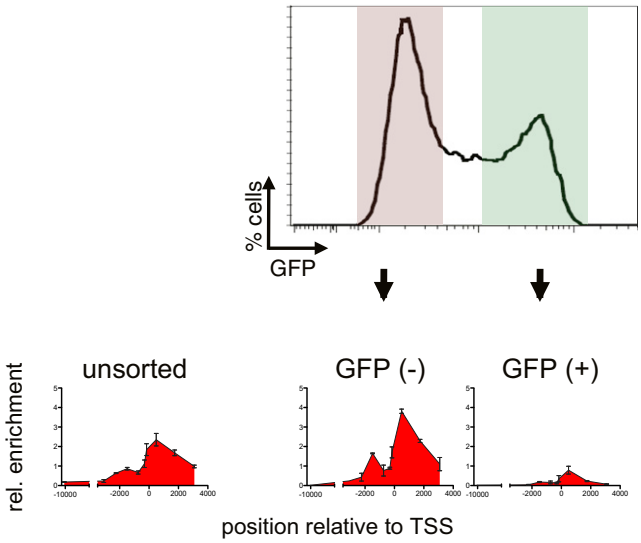

Figure S2. Establishment of H3K9me3 in FACS Sorted Populations of CiA ES Cells, Related to Figure 2

Analysis of H3K9me3 after 3 days of csHP1α recruitment in CiA ES cells. ChIPs compare relative enrichments between CiA ES cells of the unsorted, GFP-positive and GFP-negative populations. Results present an average and SEM of two independent experiments.

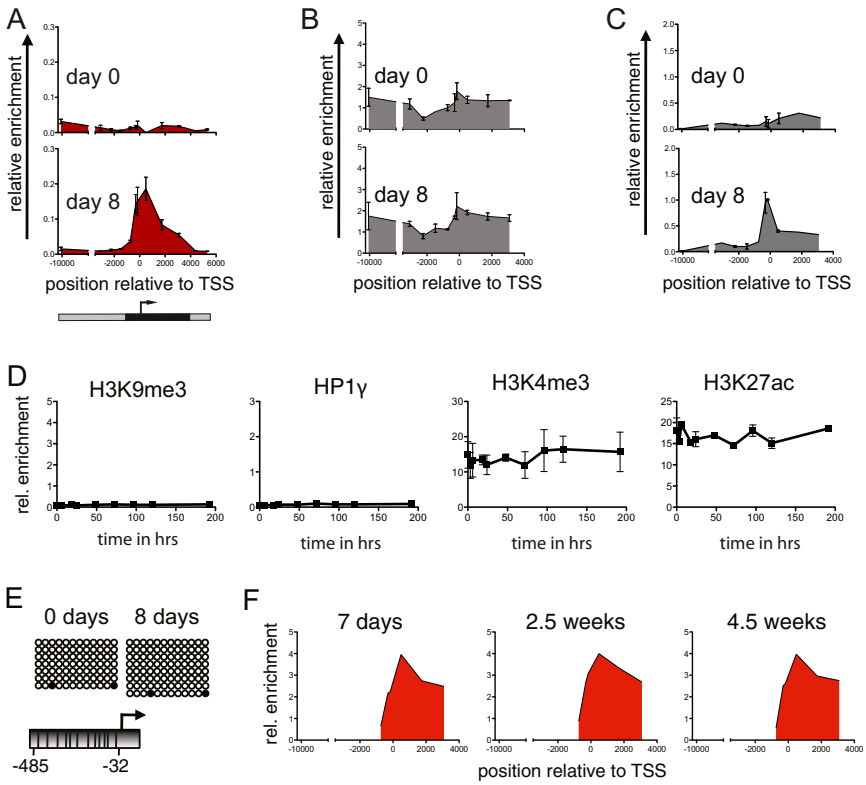

Figure S3. Chromatin structure and DNA Methylation at the CiA:Oct4 and Endogenous Alleles, Related to Figure 2

(A–C) ChIP analysis of SETDB1 binding (A), histone H3 (B) and tethered csHP1α at the *CiA:Oct4* promoter (C) before and after 8 days of csHP1α targeting in CiA ES cells. Shown are average and SEM of at least two experiments.

(D) ChIP analysis of posttranslational histone modifications and HP1γ at the endogenous *Oct4* promoter in CiA ES cells. Shown are average and SEM of at least two experiments.

(E) Bisulfite-sequencing analysis revealed that DNA methylation at the endogenous Oct4 promoter remained unchanged after 8 days of csHP1α recruitment to the *CiA:Oct4* locus.

(F) ChIP analysis of H3K9me3 at the *CiA:Oct4* locus in ES cells after csHP1α recruitment for 7 days, 2.5 weeks and 4.5 weeks.

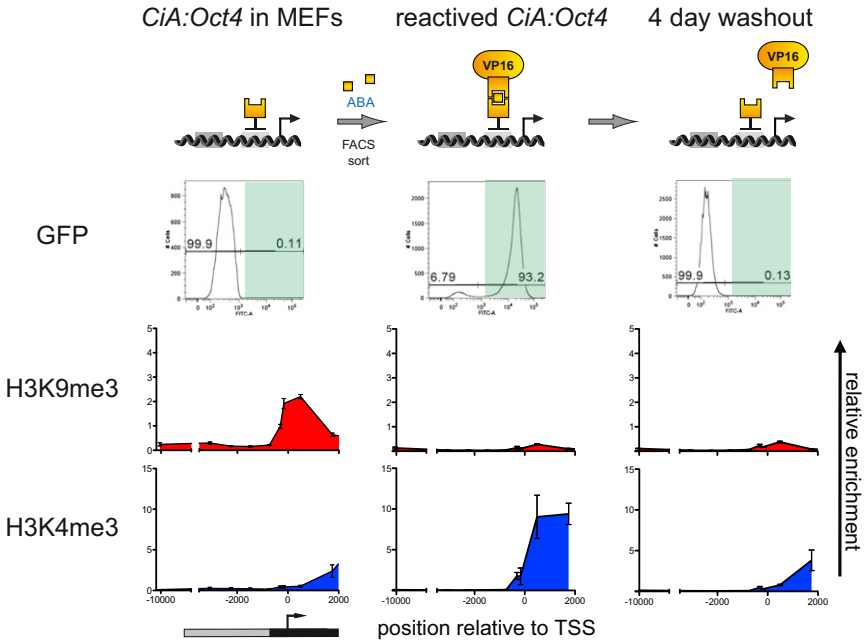

Figure S4. Addition and Removal of VP16 in CiA MEFs, Related to Figure 4

Distribution of histone modifications at the *CiA:Oct4* locus in unsorted MEFs (left panel), in GFP-positive MEFs after ABA addition (middle panel) and in GFP-negative MEFs after four days of ABA washout. ChIP results show average and SEM of two experiments.

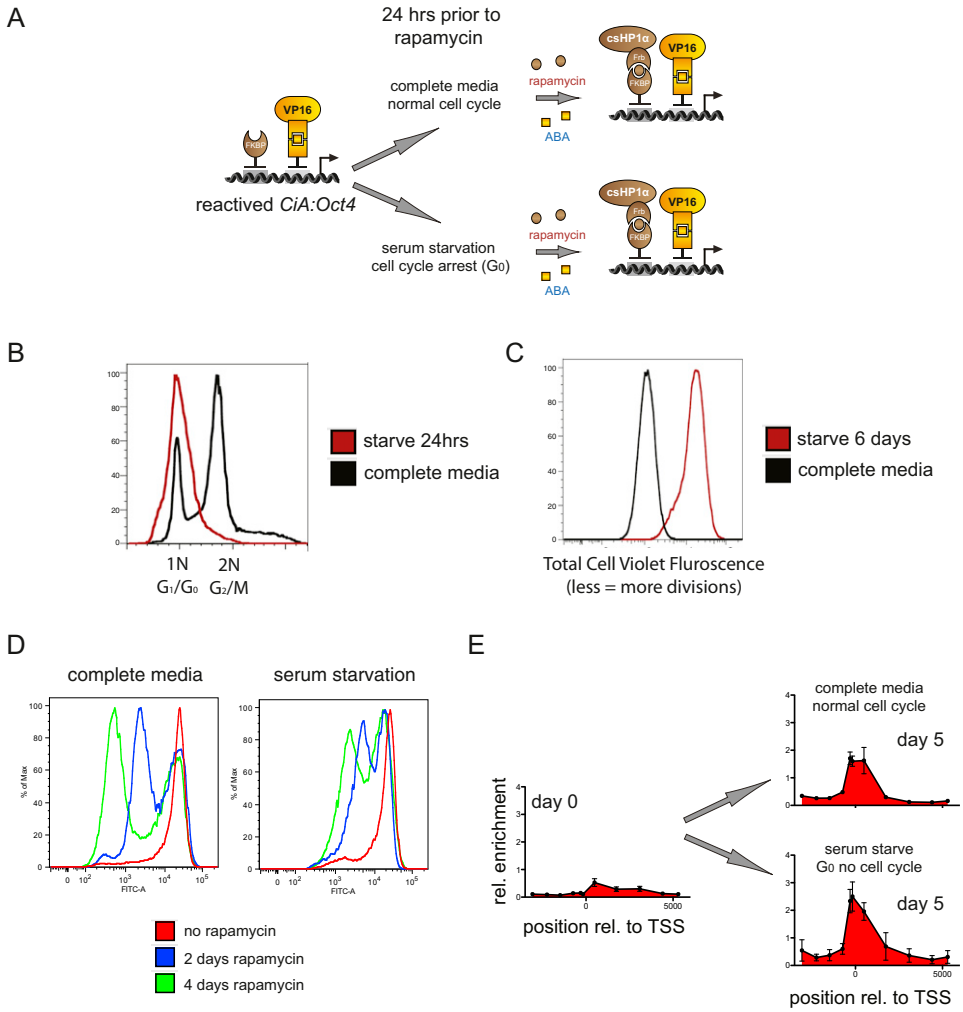

Figure S5. Contribution of Cell Division to CiA:Oct4 Repression and Heterochromatin, Related to Figure 4

(A) Schematic representation of the experimental design.

(B) 7AAD staining of CiA MEFs demonstrates effective halt of cell division after 24 hr of serum starvation (0.1% FBS) or growth in complete media (10% FBS).

(C) Cell trace violet labeling of cellular amines demonstrates difference in cell division after 6 days of starvation.

(D) FACS analysis compares GFP levels in cycling and noncycling cells after 2 and 4 days of csHP1α recruitment.

(E) ChIP analysis compares formation of steady-state H3K9me3 in cycling and noncycling CiA MEFs.

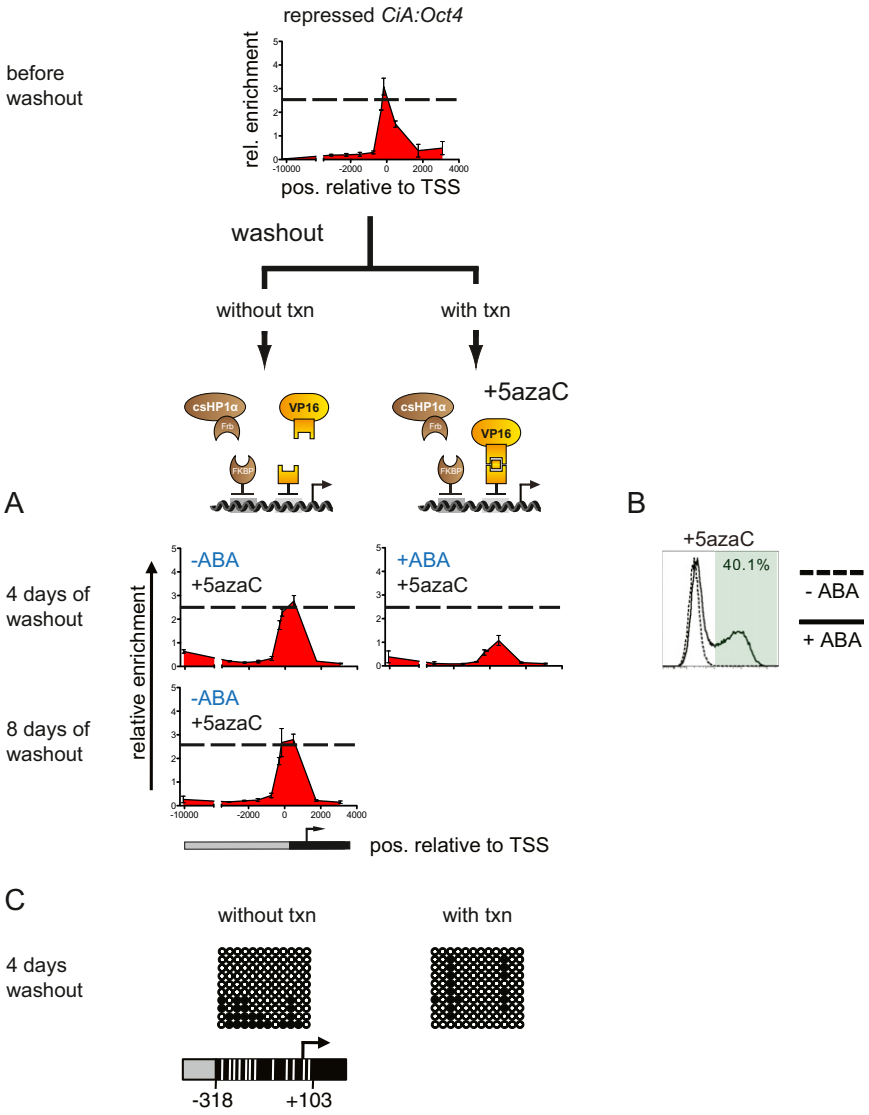

Figure S6. H3K9me3, GFP and DNA Methylation Analysis after Rapamycin Washout, Related to Figure 5

(A) Analysis of H3K9me3 after rapamycin withdrawal in the presence and absence of transcription and 5azaC. H3K9me3 ChIP enrichments present average and SEM of at least two experiments.

(B) GFP expression of CiA MEFs after four days of rapamycin washout with 5azaC comparing reactivation in the presence and absence of VP16 transcription (+ABA).

(C) Bisulfite sequencing analysis reveals CpG methylation after 4 days of rapamycin withdrawl in the presence and absence of VP16 transcription.

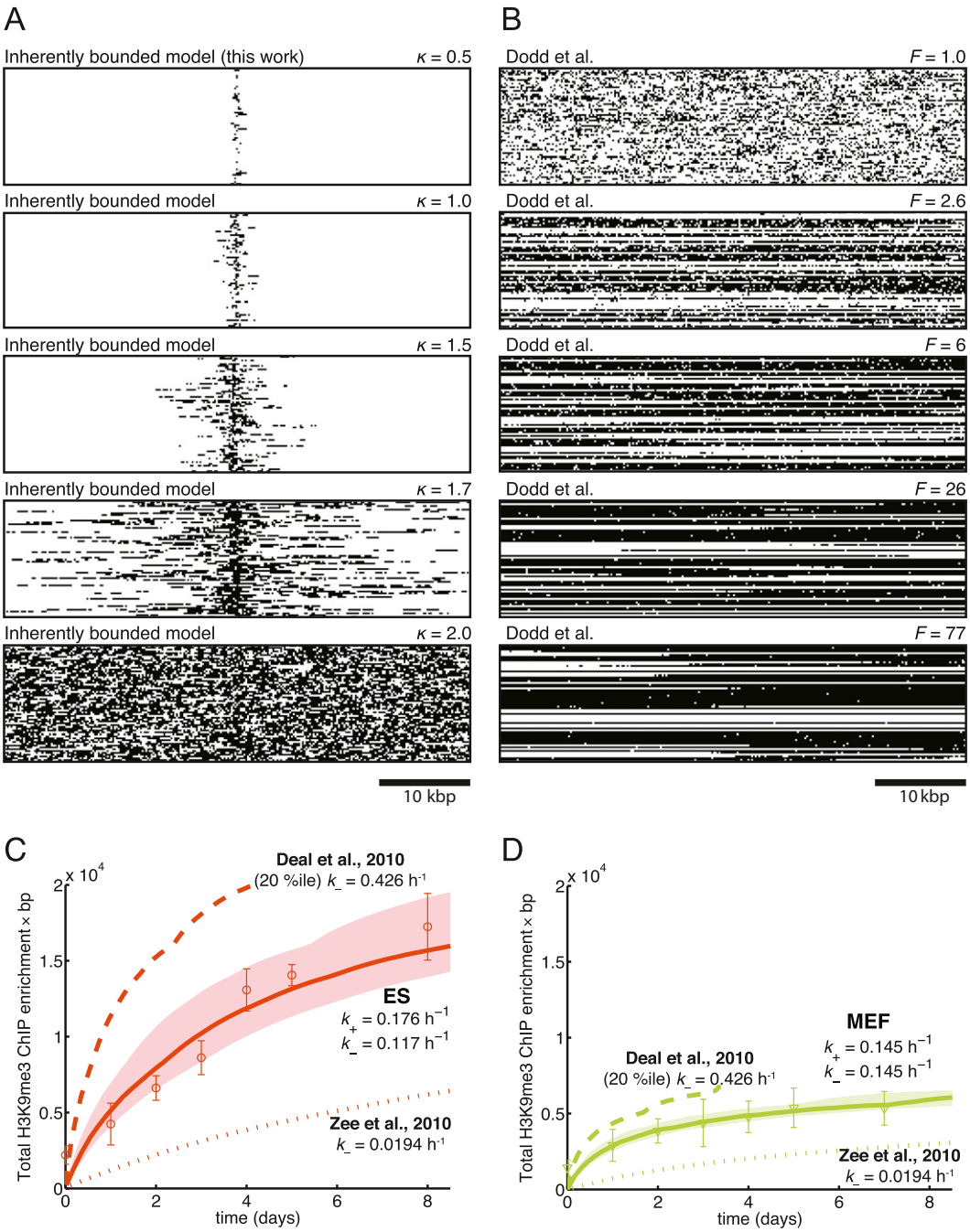

Figure S7. Kinetic Model Comparison to Literature Data, Related to Figure 6

(A) Spatial predictions of our model under varying values of κ. Each row corresponds to an individual simulation. H3K9me3-marked positions are indicated with a black pixel.

(B) Spatial distribution of marks using the model presented in Dodd et al. (2007) (reference in main text), under varying values of feedback-to-noise ratio *F*. Similarly, each row corresponds to an individual simulation.

(C) Comparison of different values for H3K9me3 turnover in ES cells. Our kinetic rates were determined by least-squares fit (solid line) of our model results to our integrated ChIP data (see Figure 6E). For comparison, we present the predicted curves from our model if k_- were obtained from published values of histone turnover. If k_- were the 20-percentile histone turnover rate in *Drosophila* S2 cells (Deal et al., 2010, reference in main text), the model would predict the upper dashed line. If instead, k_- at the CiA:Oct4 locus were the global turnover rate of H3K9me3 histones measured from HeLa cells (Zee et al., 2010, reference in main text), the model would predict the lower dotted line. Our results roughly approximate the average of these two values.

(D) Comparison of different values for H3K9me3 turnover in MEFs. The same analysis is performed in MEFs, leading to comparable results. In both ES cells and MEFs, values of k_+ are constrained by the value of κ obtained in Figure 6D).